# On the application of shooting method for determining semicontinuous distillation limit cycles


### *Authors:*

Thomas Adams II, Pranav Bhaswanth Madabhushi



*Date Submitted:* 2020-08-17

*Keywords:* Process Design, Optimization, Limit Cycle, Hybrid Dynamical System, Semicontinuous Distillation



*Abstract:*

Semicontinuous distillation is a new separation technology for distilling multicomponent mixtures. This process was designed using design methodologies with heuristic components that evolved over twenty years. However, the fundamental philosophy of these design methodologies, which involves guessing, checking and then using a black-box optimization procedure to find the values of the design variables to meet some performance criteria, has not changed. Mainly, to address the problem of having a heuristic simulation termination criterion in the black-box optimization phase, the single shooting method for semicontinuous distillation design was proposed in this study. We envision that this is a first step in the transformation of the semicontinuous distillation design process for obtaining optimal designs. We demonstrate the application of this method using two case studies, which involve the separation of hexane, heptane and octane.



*Record Type:* Preprint

*Submitted To:* LAPSE (Living Archive for Process Systems Engineering)

*Citation (overall record, always the latest version):* LAPSE:2020.0925
*Citation (this specific file, latest version):* LAPSE:2020.0925-1
*Citation (this specific file, this version):* LAPSE:2020.0925-1v1

*DOI of Published Version:* https://doi.org/https%3A//doi.org/10.1016/j.cherd.2020.05.019

# On the application of shooting method for semicontinuous distillation design

**Pranav Bhaswanth, Madabhushi, Thomas A. Adams II***

***Department of Chemical Engineering, McMaster University, 1280 Main Street West, Hamilton, Ontario, L8S 4L8, Canada***
***Email: tadams@mcmaster.ca***

Abstract

Semicontinuous distillation is a new separation technology for distilling multicomponent mixtures. This process was designed using design methodologies with heuristic components that evolved over twenty years. However, the fundamental philosophy of these design methodologies, which involves guessing, checking and then using a black-box optimization procedure to find the values of the design variables to meet some performance criteria, has not changed. Mainly, to address the problem of having a heuristic simulation termination criterion in the black-box optimization phase, the single shooting method for semicontinuous distillation design was proposed in this study. We envision that this is a first step in the transformation of the semicontinuous distillation design process for obtaining optimal designs. We demonstrate the application of this method using two case studies, which involve the separation of hexane, heptane and octane.

*Keywords*: Semicontinuous distillation, Hybrid dynamical system, Process Design, Shooting method

## 1. Introduction

Distillation is a mature technology with a plethora of possibilities for achieving cost reduction combined with energy efficiency (Kiss, 2014), thus paving the way for the development of advanced distillation technologies. Some of these advanced technologies are reactive distillation (Kiss, 2013), divided-wall column distillation (Petlyuk, 2004), cyclic distillation (Maleta et al., 2011), heat pump assisted distillation (Annakou and Mizsey, 1995), membrane distillation (Khayet, 2011). Along similar lines, Phimister and Seider, 2000, proposed the semicontinuous operation of the middle-vessel column for ternary mixture separations. This technology is an alternative to ordinary batch and continuous distillation and was called semicontinuous distillation (Adams II and Pascall, 2012). A multicomponent extension of this process was also simulated (Wijesekera and Adams, 2015a, 2015b).

In the semicontinuous distillation of multicomponent mixtures containing $c$ components, thermal separation is performed using one distillation column and $c-2$ process vessels. These process vessels are called the 'middle-vessels' (Wijesekera and Adams, 2015a) in semicontinuous distillation literature. However, throughout this article, the focus will be on the semicontinuous distillation of ternary-zeotropic mixtures, which requires only one middle-vessel. This process vessel continuously supplies a ternary mixture of time-varying composition to the distillation column through the feed stream (Figure 1). The flowrates of the distillate and bottoms streams of the distillation column are thus manipulated to control the purities of the high volatile component

(HVC) and the low volatile component (LVC) in these streams, respectively (Phimister and Seider, 2000). The composition of the contents of the middle-vessel is time-varying because a side stream from the distillation column, which contains a sufficiently high concentration of intermediate volatile component (IVC) than the contents of the middle-vessel, is continuously recycled to it.

The semicontinuous distillation of ternary mixtures has three different operating modes, which were classified based on the state of the middle-vessel (Adams and Pascall, 2012). In the separating mode, the concentration of the IVC in the middle-vessel increases and reaches the desired value. Upon reaching the desired purity value, the separating mode ends, and the discharging mode begins. In this mode, the material in the middle-vessel is discharged through the discharge stream (Figure 1), until reaching a pre-determined lower limit of liquid height. Instantaneously, material flow through the discharge stream is shut, and fresh feed to be separated is charged to the middle-vessel through the charging stream (Figure 1). The event marks the end of the discharging mode and the beginning of the charging mode. This mode ends as soon as the liquid height in the middle-vessel reaches a pre-determined upper limit. This event indicates the start of the separating mode of a new cycle, thus, making the process operation periodic.

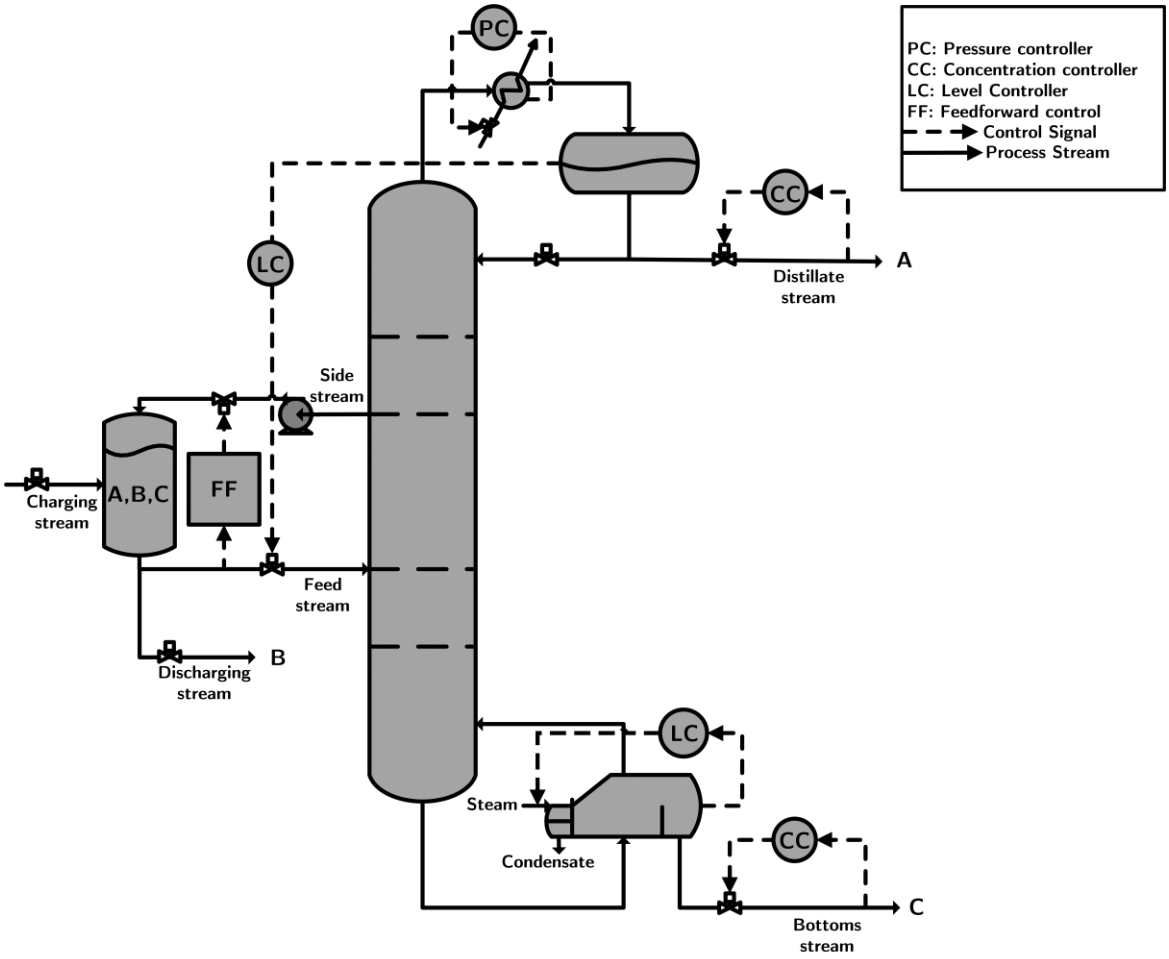


*Figure 1: Schematic of the semicontinuous distillation system for separating ternary mixtures. Reprinted with permission from Madabhushi,PranavBhaswanth, and Thomas A. Adams II. "Side stream control in*

*semicontinuous distillation." Computers & Chemical Engineering 119 (2018): 450464. Copyright 2018 Elsevier.*

The process operation within each mode is dynamic; however, the overall process operates in a steady-state called the 'limit cycle' because of its periodic behaviour (Madabhushi and Adams, 2019). A decentralized control system, which is an integral part of the process, is used to drive the column operation. This control system has multiple feedback loops to maintain the top and bottoms product purities, the reflux drum and sump levels, the column pressure and the side stream flowrate (Madabhushi and Adams, 2018).

The semicontinuous distillation process can be carried out in a traditional distillation column without any changes to the internals (Adams and Pascall, 2012), unlike cyclic distillation, which might need specially designed internals (Kiss, 2014; Toftegàrd et al., 2016). Simulation studies have shown that this process is economical at the intermediate production scale (Pascall and Adams, 2013; Wijesekera and Adams, 2015a, 2015b) while suggesting that it could be operationally flexible (Phimister and Seider, 2000).

## 2. Semicontinuous distillation design

In this section, we first review the evolution of the design methodologies used for the design of semicontinuous distillation of ternary mixtures. Later we expound some of the philosophical underpinnings of these design methodologies, which fundamentally differ from the proposed approach.

The seminal paper on the semicontinuous distillation of ternary mixtures introduced the first design methodology. It is a shortcut design procedure that adapted the Fenske-Underwood equations to determine the minimum reflux ratio and the number of stages (Phimister and Seider, 2000). These equations were applied, assuming that the system operates at a pseudo-steady state when the column is at, or near, the total reflux state during the dynamic operation within an operating mode (Phimister and Seider, 2000). Furthermore, using this pseudo-steady state, the trays were sized, and the column internal flowrates were determined. The internal flowrates were used to estimate the column diameter while ensuring hydraulically feasible (no flooding and weeping) column operation at this state (Phimister and Seider, 2000). The parameters of the controllers in the decentralized control system were tuned to ensure proper control performance (setpoint tracking and disturbance rejection) during the dynamic operation. Performance testing of the design is carried out by simulating the system, which entails numerical integration of the system's model equations until reaching a limit cycle. We call this the original design methodology.

Later, Pascall and Adams, 2013, proposed a completely new design methodology. They used the steady-state of a continuous distillation system that separates the low and high volatile components to the desired purity values to find the design of the semicontinuous distillation system. This state happens to closely represent the dynamic operation of the semicontinuous distillation system at the beginning of the separating mode (Pascall and Adams, 2013). The continuous distillation system was derived from the semicontinuous distillation system by merely not recycling the side stream to the middle-vessel. The values of the number of trays, feed and side stream stage locations, and the reflux and reboil rates were determined such that the continuous

distillation system operates in the desired steady-state. Based on the flowrates at this steady-state, equipment sizes for semicontinuous distillation were determined. Then using the sized equipment and the steady-state as the initial state, dynamic simulations of semicontinuous distillation were run. These simulations were carried out for different combinations of controller tuning parameter values to find a limit cycle. Then a black-box optimization procedure was used to find the tuning parameter values that minimized the total annualized cost per production rate of a product. This design procedure was called the sequential design methodology by Meidanshahi and Adams, 2016.

Subsequently, more changes were made by Madabhushi and Adams, 2019, to the way the steady-state of the continuous distillation system was chosen. Discovery that the cycle time (period of the limit cycle) is sensitive to the choice of this steady-state by Madabhushi et al., 2018, led to the development of a new design methodology. This design procedure introduced an iterative method to change the steady-state at which a slightly modified version of the previously described continuous distillation system operates (Madabhushi and Adams, 2019). In the designs obtained by using this method, the material is recycled to the middle vessel through the side stream at a maximum possible flowrate (Madabhushi and Adams, 2019). Moreover, at the same time, the column is operated in a hydraulically feasible limit cycle (Madabhushi and Adams, 2019). Equipment in the semicontinuous distillation system were again sized based on the steady-state flowrates. This design methodology was called the backstepping design methodology (Madabhushi and Adams, 2019).

As the first step of this design methodology, the ratio of side stream to feed flowrate of the modified continuous distillation system was chosen to be approximately 1.0. This ratio is a degree of freedom in the design of this system. The other degrees of freedom of this system were determined such that this system operates in a steady-state that satisfies the hydraulic feasibility constraints. As stated before, based on the flowrate values at this steady-state, the equipment sizes for semicontinuous distillation were determined. Then using the sized equipment and the steady-state as the initial state, dynamic simulations of semicontinuous distillation were run. These simulations were carried out at different latin hypercube sampling points. The points were sampled from the space formed by the controller tuning parameters, reflux rate, the initial side stream flowrate, and the initial reboil rate. Initial here refers to the values of these variables at the beginning of the semicontinuous distillation simulation. A different steady-state was chosen by lowering the ratio of side stream to feed flowrate if desirable limit cycles cannot be found at any of these sampling points. A desirable limit cycle is hydraulically feasible, where components were separated to the desired purity values. This process is repeated until at least one desired limit cycle is found at any of the sampled points. After finding desirable limit cycles, a black-box optimization procedure was used to find the design that minimized the total annualized cost per production rate of a product.

The underlying philosophy behind the original, sequential and backstepping design methodologies is that many simulations of the semicontinuous distillation system were performed first to find a feasible design. Then an optimal design is sought after using black-box optimization. In these design procedures, although better heuristic knowledge is incorporated to yield improved designs (in terms of cost benefits), the process is ultimately still a guess and check procedure. A large number of otherwise avoidable simulations might be necessary to reject parts of the design space, thus requiring a significant amount of CPU time (typically of the order of weeks) for design

optimization. Moreover, since a black-box optimization procedure was used in these design methodologies, the guarantee of reaching a global or even a local optimum did not exist.

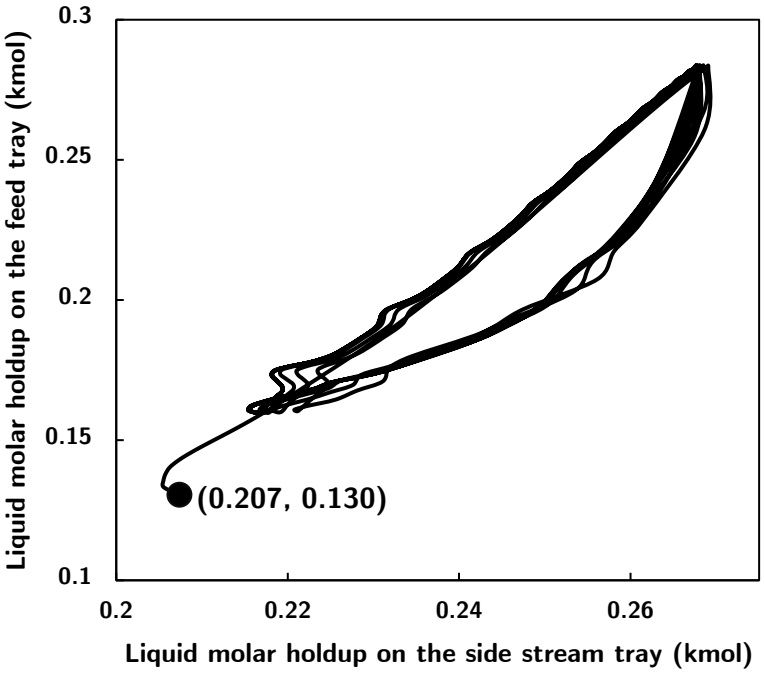


*Figure 2: Phase plane (2-D) of hexane, heptane and octane semicontinuous distillation. The trajectory that settles on the limit cycle starting from the initial state at (0.207, 0.130)*

In the simulation of the semicontinuous distillation process, the accurate dynamic model of the system that includes operating mode transitions is numerically integrated, starting from an initial state that does not lie on the limit cycle. Therefore the system trajectory passes through a transient phase before settling on the limit cycle (Figure 2) (Seydel, 2010). The length of this transient phase is dependent on the design and the initial state (Figure 3). Termination of the numerical integration, during simulation, is based on visual confirmation that a limit cycle is reached. However, visually tracking trajectories to ascertain that a limit cycle is attained is not possible in the black-box optimization phase, which necessitates having a heuristically chosen termination criterion. For example, we chose the $10^{th}$ cycle to be the limit cycle after extensively studying the systems presented in Madabhushi and Adams, 2019, for different designs.

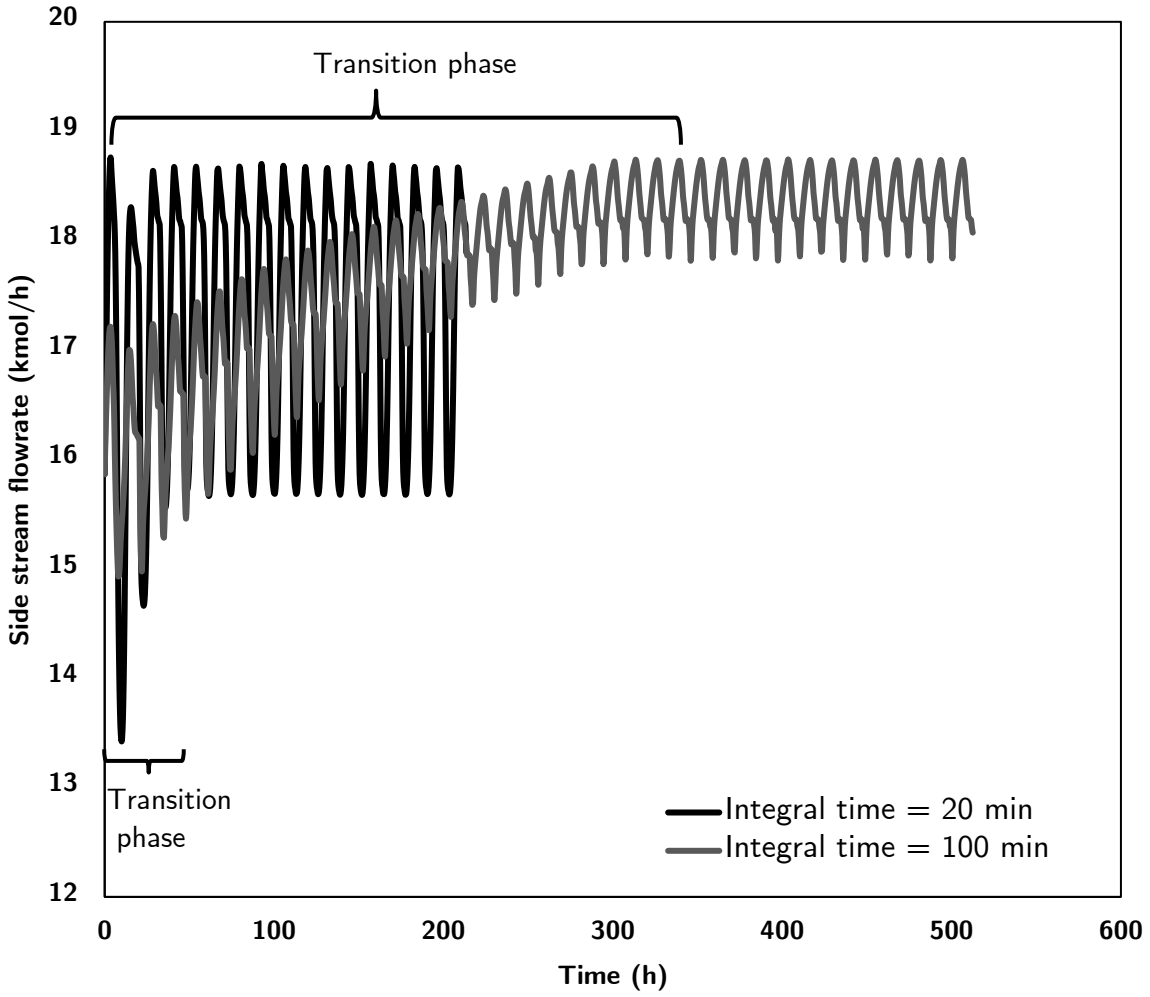


*Figure 3: Different lengths of the transition phase when the controller tuning parameter of the side stream flowrate controller (Proportional-Integral) is changed in the semicontinuous distillation of hexane, heptane and octane.*

In this paper, for the first time, we demonstrate the application of the shooting method to precisely locate the limit cycle of the semicontinuous distillation system. This method of simulating the process addresses the problem of using a heuristic simulation termination criterion. The shooting method is particularly suitable for use in combination with any of the gradient-based optimization methods to find the optimal semicontinuous distillation design. We envision that this systematic design method will have the potential for reducing CPU times significantly to obtain the optimal design. It also immediately opens up opportunities to find guaranteed local optimal designs with prospects in the future for finding a globally optimal design.

We present the two-point boundary value formulation of the semicontinuous distillation system with non-separable periodic boundary conditions (Ascher and Petzold, 1998). We numerically solve this boundary value problem (BVP) using the shooting method, which converts the BVP to an initial value problem (IVP). Then the zeros of the boundary conditions are calculated to find the limit cycle (Ascher and Petzold, 1998; Parker et al., 1989). The application of this method is

demonstrated using two case studies to illustrate the paradigm shift in the way the semicontinuous distillation process will be designed in the future.

## 3. The mathematical model of the process

The non-linear dynamic model of semicontinuous distillation is embedded with events that trigger discrete changes to the equations in this model. These types of systems can be modelled using the hybrid (discrete/continuous) systems mathematical framework (Barton and Lee, 2004). The mathematical model of the process is described subsequently using the language of this framework.

The hybrid automaton representation of the process has three distinct modes ($\{\mu_1, \mu_2, \mu_3\}$), each of which represents a process operating mode. The nonlinear dynamic model of the process within each mode includes the equation systems of the distillation column, the middle-vessel, and the control system. This dynamic model describes the continuous evolution of the system in the time interval $[t_{i-1}(\boldsymbol{p_d}, \boldsymbol{p_r}), t_i(\boldsymbol{p_d}, \boldsymbol{p_r}))$, in mode $\mu_i$, where $\boldsymbol{p_d}$ represents the vector of design variables that take discrete values (discrete design variables), and $\boldsymbol{p_r}$ represents the vector of design variables that take real values (real design variables). A general representation of the non-linear dynamic model of the semicontinuous distillation process in mode $\mu_i$ as a system of semi-explicit differential-algebraic equations (DAEs) is given below,

$$\dot{\boldsymbol{z}}^{(\mu_i)}(t, \boldsymbol{p_d}, \boldsymbol{p_r}) = \begin{bmatrix} \boldsymbol{\Psi}_{cc}\left(\boldsymbol{z}^{(\mu_i)}, \boldsymbol{y}^{(\mu_i)}(t, \boldsymbol{p_d}, \boldsymbol{p_r}), \boldsymbol{p_d}, \boldsymbol{p_r}\right) \\ \boldsymbol{\Psi}_{mv}^{(\mu_i)}\left(\boldsymbol{z}^{(\mu_i)}, \boldsymbol{y}^{(\mu_i)}(t, \boldsymbol{p_d}, \boldsymbol{p_r}), \boldsymbol{p_d}, \boldsymbol{p_r}\right) \end{bmatrix}$$

$$\boldsymbol{0} = \begin{bmatrix} \boldsymbol{\Phi}_{cc}\left(\boldsymbol{z}^{(\mu_i)}, \boldsymbol{y}^{(\mu_i)}(t, \boldsymbol{p_d}, \boldsymbol{p_r}), \boldsymbol{p_d}, \boldsymbol{p_r}\right) \\ \boldsymbol{\Phi}_{mv}^{(\mu_i)}\left(\boldsymbol{z}^{(\mu_i)}, \boldsymbol{y}^{(\mu_i)}(t, \boldsymbol{p_d}, \boldsymbol{p_r}), \boldsymbol{p_d}, \boldsymbol{p_r}\right) \end{bmatrix} \quad i = \{1, 2, 3\} \qquad (1)$$

where $\boldsymbol{z}$ represents the vector of differential states, $\boldsymbol{y}$ represents the vector of algebraic states. In the DAE system, $\boldsymbol{\Psi}_{cc}$, and $\boldsymbol{\Phi}_{cc}$ represent the system of differential and algebraic equations, respectively, of the column and the control system together. And, $\boldsymbol{\Psi}_{mv}^{(\mu_i)}$, and $\boldsymbol{\Phi}_{mv}^{(\mu_i)}$ represent the differential and algebraic equations, respectively, of the middle vessel in mode $\mu_i$. Note that the column and control system DAEs are not mode dependent. State-dependent events, which cause instantaneous transitions from mode, $\mu_i$, to mode, $\mu_j$, at the time, $t_i$, trigger switches in the equations describing the middle-vessel only. These state-dependent discrete events and the associated discrete control actions taken are listed below,

(1) **Separating mode ($\mu_1$) to discharging mode ($\mu_2$) transition**:
*Event*: mole fraction of the IVC in the middle-vessel ($x_{mv,IVC}^{(\mu_1)}(t, \boldsymbol{p_d}, \boldsymbol{p_r})$) is at the desired purity value ($x_{mv,IVC}^{desired}$), i.e., the event occurs when the transition condition $\Omega_{\mu_1}^{\mu_2}(t, \boldsymbol{p_d}, \boldsymbol{p_r}) = 0$ is met, where $\Omega_{\mu_1}^{\mu_2}(t, \boldsymbol{p_d}, \boldsymbol{p_r}) \coloneqq x_{mv,IVC}^{(\mu_1)}(t, \boldsymbol{p_d}, \boldsymbol{p_r}) - x_{mv,IVC}^{desired}$. Here, $\Omega_{\mu_1}^{\mu_2}$ is the condition required to transition from mode $\mu_1$ to mode $\mu_2$ at $t_1(\boldsymbol{p_d}, \boldsymbol{p_r})$.
*Control action*: Fully open the discharge stream valve (Figure 1).

(2) **Discharging mode ($\mu_2$) to charging mode ($\mu_3$) transition**:
*Event*: The height of the liquid in the middle-vessel ($h_{mv}^{(\mu_2)}(t, \boldsymbol{p_d}, \boldsymbol{p_r})$) is at the predetermined lower limit ($h_v^l$), i.e., the event occurs when the transition condition $\Omega_{\mu_2}^{\mu_3}(t, \boldsymbol{p_d}, \boldsymbol{p_r}) = 0$ is met, where $\Omega_{\mu_2}^{\mu_3}(t, \boldsymbol{p_d}, \boldsymbol{p_r}) \coloneqq \left(h_{mv}^{(\mu_2)}(t, \boldsymbol{p_d}, \boldsymbol{p_r}) - h_{mv}^l\right)$. Here, $L_{\mu_2}^{\mu_3}$ is the condition required to transition from mode $\mu_2$ to mode $\mu_3$ at $t_2(\boldsymbol{p_d}, \boldsymbol{p_r})$. This condition ensures that the downstream pump, which feeds the distillation column, does not cavitate.
*Control action*: Fully close the discharge stream valve (Figure 1), and fully open the charging stream valve (Figure 1).

(3) **Charging mode ($\mu_3$) to separating mode ($\mu_1$) transition**:
*Event*: the height of the liquid in the middle-vessel is at the predetermined upper limit ($h_{mv}^u$), i.e., the event occurs when the transition condition $\Omega_{\mu_3}^{\mu_1}(t, \boldsymbol{p_d}, \boldsymbol{p_r}) = 0$ is met, where $\Omega_{\mu_3}^{\mu_1}(t, \boldsymbol{p_d}, \boldsymbol{p_r}) \coloneqq \left(h_{mv}^{(\mu_3)}(t, \boldsymbol{p_d}, \boldsymbol{p_r}) - h_{mv}^u\right)$. Here, $\Omega_{\mu_3}^{\mu_1}$ is the condition required to transition from mode $\mu_3$ to mode $\mu_1$ at $t_3(\boldsymbol{p_d}, \boldsymbol{p_r})$. This condition ensures the safety of the process operation.
*Control action*: Fully close the charging stream valve (Figure 1).

Note here that the transition times, $t_1(\boldsymbol{p_d}, \boldsymbol{p_r})$, $t_2(\boldsymbol{p_d}, \boldsymbol{p_r})$, and $t_3(\boldsymbol{p_d}, \boldsymbol{p_r})$ at which the transition conditions, $\Omega_{\mu_1}^{\mu_2}(t, \boldsymbol{p_d}, \boldsymbol{p_r})$, $\Omega_{\mu_2}^{\mu_3}(t, \boldsymbol{p_d}, \boldsymbol{p_r})$, and $\Omega_{\mu_3}^{\mu_1}(t, \boldsymbol{p_d}, \boldsymbol{p_r})$ are satisfied are unknown *a priori* since the events are state-dependent. As the process is periodic, it follows this particular fixed mode sequence: $\{\mu_1, \mu_2, \mu_3, \mu_1\}$, which is called the hybrid mode trajectory ($T_\mu$) (Barton and Lee, 2004). In this paper, we consider that the operation starts at the beginning of the separating mode and again ends here.

The contiguous closed time intervals $[t_{i-1}(\boldsymbol{p_d}, \boldsymbol{p_r}), t_i(\boldsymbol{p_d}, \boldsymbol{p_r})]$ in which the modes evolve are called epochs ($\theta_i$) (Barton and Lee, 2004) and a finite sequence of epochs ($\{E_i, i \in 1 \text{ to } n_e\}$) is known as a hybrid time trajectory (Barton and Lee, 2004). Based on the hybrid mode trajectory and starting from the beginning of $\mu_1$, the semicontinuous distillation process has four epochs, where $\theta_1 \in [t_0(\boldsymbol{p_d}, \boldsymbol{p_r}), t_1(\boldsymbol{p_d}, \boldsymbol{p_r})]$, $\theta_2 \in [t_1(\boldsymbol{p_d}, \boldsymbol{p_r}), t_2(\boldsymbol{p_d}, \boldsymbol{p_r})]$, $\theta_3 \in [t_2(\boldsymbol{p_d}, \boldsymbol{p_r}), t_3(\boldsymbol{p_d}, \boldsymbol{p_r})]$, and $\theta_4 \in [t_3(\boldsymbol{p_d}, \boldsymbol{p_r}), t_3(\boldsymbol{p_d}, \boldsymbol{p_r})]$, and the hybrid time trajectory is $T_t = \{\theta_1, \theta_2, \theta_3, \theta_4\}$. The last epoch only ensures that the system transitions back to the beginning of mode $\mu_1$, and thus the time elapsed in the mode is zero.

The DAE system in each mode is initialized using transition functions, which are defined to relate variables in the mode $\mu_i$ to variables in the subsequent mode $\mu_j$ (Galán et al., 1999). In the hybrid model of the semicontinuous distillation system, the transition function ensures the continuity of the differential and algebraic state variables when transitioning from one mode to another. Thus, the function initializes the DAE system of the subsequent mode after the mode transition with the values of these variables at the event time.

$$\boldsymbol{\Theta}_{\boldsymbol{z}_{\mu_i}}^{\mu_j}(t, \boldsymbol{p_d}, \boldsymbol{p_r}) \coloneqq \boldsymbol{z}^{(\mu_i)}\left(\boldsymbol{p_d}, \boldsymbol{p_r}, t_i(\boldsymbol{p_d}, \boldsymbol{p_r})\right) - \boldsymbol{z}^{(\mu_j)}\left(\boldsymbol{p_d}, \boldsymbol{p_r}, t_i(\boldsymbol{p_d}, \boldsymbol{p_r})\right) = 0 \quad (2)$$

$$\boldsymbol{\Theta}_{\boldsymbol{y}_{\mu_i}}^{\mu_j}(t, \boldsymbol{p_d}, \boldsymbol{p_r}) \coloneqq \boldsymbol{y}^{(\mu_i)}\left(\boldsymbol{p_d}, \boldsymbol{p_r}, t_i(\boldsymbol{p_d}, \boldsymbol{p_r})\right) - \boldsymbol{y}^{(\mu_j)}\left(\boldsymbol{p_d}, \boldsymbol{p_r}, t_i(\boldsymbol{p_d}, \boldsymbol{p_r})\right) = 0 \quad (3)$$

where $i \neq j$ and $i < j$, and $\boldsymbol{\Theta}_{\boldsymbol{z}_{\mu_i}}^{\mu_j}$ represents the transition functions related to the differential variables, and $\boldsymbol{\Theta}_{\boldsymbol{y}_{\mu_i}}^{\mu_j}$ represents the transition functions related to the algebraic variables.

### 3.1 The dynamic model of the semicontinuous distillation system

The sub-systems in the semicontinuous distillation system, which comprises of the distillation column, the middle-vessel, and the control system were modelled using the principle of mass conservation, vapour-liquid equilibrium relationship, tray hydraulics and control laws.

The distillation column dynamic model was well-studied in the literature by different authors, such as Gani et al., 1986, Flatby et al., 1994, Bansal et al., 2002, for different applications such as start-up, control, and design optimization. Different assumptions were made in each of the studies depending on the application of the model. In this study, we used several classical simplifying assumptions, since the purpose of the study is to demonstrate the application of the single shooting method to use this procedure later for finding the optimal design of the process.

The assumptions that were used are adiabatic column operation, constant top stage pressure with a constant pressure drop across a stage, negligible vapour-holdup, perfect mixing on the trays, 100% Murphee tray efficiency, and total condenser with saturated liquid outlet conditions. Also, we assume constant molar overflow, which yields from energy balance, $V_n = V_{n-1}$ (Skogestad, 1997), where $n$ represents the stage number which is assigned from the top of the column, and $V$ is the total vapour flowrate. The dynamic model of the column, however, considers the liquid flow dynamics by the inclusion of the Francis Weir Equation. The mass balance equations of the column were expressed as differential equations at each stage for each component, while the phase equilibrium and the hydraulic models are algebraic.

***Column Material Balances***

The component material balance equations of the total condenser stage, which includes the reflux drum ($n = 1$) are compactly represented below:

$$\frac{dm_{1,c}}{dt} = v_{2,c} - l_{1,c} - d_c, \;\; c = \{\text{HVC}, \text{IVC}, \text{LVC}\} \tag{4}$$

where,

$m_{1,c}$ is the liquid molar holdup of component $c$ on stage 1

$l_{1,c}$ is the molar reflux rate of component $c$ leaving stage 1

$v_{2,c}$ is the vapour molar flowrate of component $c$ entering stage 1

$d_c$ is the distillate molar flowrate of component $c$ leaving stage 1.

The component material balance equations of stages $n = \{2,3, \dots, N_s - 1\}$, where $N_s$ is the total number of stages, are compactly represented below:

$$\frac{dm_{n,c}}{dt} = l_{n-1,c} + v_{n+1,c} - l_{n,c} - v_{n,c} + \zeta f_c - \varsigma s_c, \;\; c = \{\text{HVC}, \text{IVC}, \text{LVC}\} \tag{5}$$

where,

$m_{n,c}$ is the liquid molar holdup of component $c$ on stage $n$

$l_{n,c}$ is the liquid molar flowrate of component $c$ leaving stage $n$

$v_{n,c}$ is the vapour molar flowrate of component $c$ leaving stage $n$

$f_c$ is the molar flowrate of component $c$ in the liquid feed

$s_c$ is the molar flowrate of component $c$ in the liquid side stream

$$\zeta = \begin{cases} 1, & n = n_f \\ 0, & else \end{cases}$$

$$\varsigma = \begin{cases} 1, & n = n_s \\ 0, & else \end{cases}$$ ($n_f$ is the feed stage location, $n_s$ is the side stream stage location)

Finally, the component material balance equations of the partial reboiler stage ($n = N_s$) are compactly represented below:

$$\frac{dm_{N_s,c}}{dt} = l_{N_s-1,c} - b_c - v_{N_s,c}, \ c = \{\text{HVC}, \text{IVC}, \text{LVC}\} \quad (6)$$

where,

$m_{N_s,c}$ is the liquid molar holdup of component $c$ on stage $N_s$

$l_{N_s-1,c}$ is the liquid molar flowrate of component $c$ entering the stage $N_s$

$v_{N_s,c}$ is the vapour molar flowrate of component $c$ leaving the stage $N_s$

$b_c$ is the bottoms molar flowrate of component $c$ leaving the stage $N_s$.

***Column - Vapour Liquid Equilibrium***

On each stage of the distillation column, the vapour and the liquid phases are in contact and are assumed to be at equilibrium throughout the periodic operation in this article. The phase equilibrium was modelled using Raoult's Law and the Antoine equation.

$$K_c(T_n, P_n) = \frac{y_{n,c}}{x_{n,c}} \quad (7)$$

$$K_c(T_n, P_n) = \frac{P_c^{sat}(T_n)}{P_n} \quad (8)$$

$$\ln\left(P_c^{sat}(T_n)\right) = A_c + \frac{B_c}{T_n} + C_c \log(T_n) + D_c T_n^{E_c} \quad (9)$$

where,

$K_c(T_n, P_n)$ is the phase equilibrium ratio of component $c$ on stage $n$

$y_{n,c}$ is the mole fraction of component $c$ in the vapour leaving stage $n$

$x_{n,c}$ is the mole fraction of component $c$ in the liquid leaving stage $n$

$P_c^{sat}(T_n)$ is the vapour pressure of $c$ on stage $n$

$T_n$ is the temperature of the stage $n$

$P_n$ is the pressure of the stage $n$

$A_c$, $B_c$, $C_c$, $D_c$, $E_c$ are the Antoine parameters for component $c$.

The mole fraction of the components in the vapour streams and the liquid streams are normalized using the following set of equations, where $L_n$ is the total flowrate of liquid leaving stage $n$, $V_n$ is the total flowrate of vapour leaving stage $n$, and $M_n$ is the total molar holdup of liquid on stage $n$.

$$\sum_c x_{n,c} = \sum_c y_{n,c} = 1 \tag{10}$$

$$l_{n,c} = x_{n,c} L_n \tag{11}$$

$$v_{n,c} = y_{n,c} V_n \tag{12}$$

$$\frac{m_{n,c}}{M_n} = \frac{l_{n,c}}{L_n} \tag{13}$$

***Column - Tray Hydraulics***

The Francis weir equation (Perry and Green, 2013; Prokopakis and Seider, 1983) was used to predict the total liquid flowrate over the weir based on the weir height ($h_{weir}$), weir length ($L_{weir}$), tray cross-sectional area ($A_{Tray}$), the density of liquid on tray $n$ ($\rho_n^{liq}(x_{n,c}, T_n, P_n)$), and the gravitational constant ($g$). We assume that the weir used is a segmental weir.

$$M_n = A_{Tray} \rho_n^{liq}(x_{n,c}, T_n, P_n) \left[ h_{weir} + 1.41 \left( \frac{L_n}{\rho_n^{liq}(x_{n,c}, T_n, P_n) L_{weir} \sqrt{g}} \right)^{2/3} \right] \tag{14}$$

The density of liquid on stage $n$ is approximated using the Rackett equation (Green and Southard, 2019),

$$\ln\left( \frac{1}{\rho_{n,c}^{liq}(x_{n,c}, T_n, P_n)} \right) = \ln\left( \frac{R_{gas} T_c^{cr}}{P_c^{cr}} \right) + \left[ 1 + \left( 1 - \frac{T_n}{T_c^{cr}} \right)^{2/7} \right] \ln(Z_c^{Ra}) \tag{15}$$

$$\rho_n^{liq}(x_{n,c}, T_n, P_n) = \sum_c x_{n,c} \rho_{n,c}^{liq}(x_{n,c}, T_n, P_n) \tag{16}$$

where,

$R_{gas}$ is the ideal gas constant

$T_c^{cr}$ is the critical temperature of component $c$

$P_c^{cr}$ is the critical pressure of component $c$

$Z_c^{Ra}$ is the Rackett compressibility factor of component $c$.

***Control Sub-System***

The semicontinuous distillation control subsystem has five different feedback control loops, which are:

(1) Distillate concentration control loop

(2) Bottoms concentration control loop

(3) Reflux drum level control loop

(4) Sump level control loop

(5) Side stream flowrate control loop

The controller used in all these feedback control loops is a proportional-integral (PI) controller. In this paper, we use the parallel form of the PI control law, which is

$$u(t) = u_{bias} \mp K_p e(t) \mp K_i \int_0^t e(\tau) d\tau \quad (17)$$

where,

$u(t)$ is the manipulated variable

$u_{bias}$ is the controller bias

$K_p$ is the proportional gain

$K_i$ is the integral gain

$e(t)$ is the error (Setpoint – Process Variable value at time $t$).

The error is further defined as follows,

$$e(t) = SP - PV(t) \quad (18)$$

where, $SP$ is the setpoint, and $PV(t)$ is the process variable value at time $t$. The negative sign in the equation comes into play when the controller is reverse-acting and not direct-acting. Instead of directly using the form of the control law presented in (13), the following differential form of the control law is used, where $I$ is the differential state.

$$\frac{dI}{dt} = e(t) \tag{19}$$

$$u(t) = u_{bias} \mp K_p e(t) \mp K_i I \tag{20}$$

*Table 1: The table shows the manipulated variables, setpoints, and the process variables in the different control loops.*

| | $\boldsymbol{u(t)}$ | $\boldsymbol{SP}$ | $\boldsymbol{PV(t)}$ |
|---|---|---|---|
| **Distillate concentration control loop** | Distillate flowrate ($d(t)$) | Desired mole fraction of HVC on stage 1 ($x_{1,HVC}^{desired}$) | Mole fraction of HVC on stage 1 ($x_{1,HVC}(t)$) |
| **Bottoms concentration control loop** | Bottoms flowrate ($b(t)$) | Desired mole fraction of HVC on stage $N_s$ ($x_{N_s,LVC}^{desired}$) | Mole fraction of HVC on stage $N_s$ ($x_{N_s,LVC}(t)$) |
| **Reflux drum level control loop** | Feed flowrate to the column ($F(t)$) | Desired height of liquid in the reflux drum ($h_{reflux}^{desired}$) | Height of liquid in the reflux drum ($h_{reflux}(t)$) |
| **Sump level control loop** | Reboil rate ($V_{N_s}(t)$) | Desired height of liquid in the sump ($h_{sump}^{desired}$) | Height of liquid in the sump ($h_{sump}(t)$) |
| **Side stream flowrate control loop** | Side stream flowrate ($S(t)$) | Feed stream component IVC flowrate ($f_{n_f,IVC}(t)$) | Side stream component IVC flowrate ($s_{n_s,IVC}(t)$) |

From Table 1, notice that the modified-ideal side draw recovery arrangement is used to change the setpoint of the side stream flowrate controller (Madabhushi and Adams, 2018). Also, note that it is ensured that the manipulated variables are clipped between desired lower and upper bound values.

The height of the liquid in the reflux drum (stage 1) and sump (stage $N_s$) are obtained using the following relationships, where $A_{reflux}$ is the area of the reflux drum and $A_{sump}$ is the area of the sump,

$$h_{reflux} = \frac{M_1}{\rho_1^{liq}(x_{1,c}, T_1, P_1)\, A_{reflux}} \tag{21}$$

$$h_{sump} = \frac{M_{N_S}}{\rho_{N_S}^{liq}(x_{N_S,c}, T_{N_S}, P_{N_S})\, A_{sump}} \tag{22}$$

***Middle-Vessel - Material Balances***

The mode-specific component mass balance equations of the middle vessel are represented compactly as shown here,

$$\frac{dm_{mv,c}}{dt} = s_{n_s,c} + \alpha f_{charge,c} - f_{n_f,c} - \beta f_{discharge,c},\ c = \{\text{HVC}, \text{IVC}, \text{LVC}\} \quad (23)$$

where,

$m_{mv,c}$ is the liquid molar holdup of component $c$ in the middle vessel

$f_{charge,c}$ is the liquid flowrate of component $c$ in the charging stream (Figure 1)

$f_{discharge,c}$ is the liquid flowrate of component $c$ in the discharge stream (Figure 1)

$$\alpha = \begin{cases} 1, & T_\mu = \mu_3 \\ 0, & else \end{cases}$$

$$\beta = \begin{cases} 1, & T_\mu = \mu_2 \\ 0, & else \end{cases}$$

From the material balances of the column and the middle-vessel, the vapour liquid equilibrium relationships, the tray hydraulics, and the PI controller equations, we can gather the following: the differential variables ($\boldsymbol{z}$) are all the liquid molar holdups ($m_{n,c}$ and $m_{mv,c}$) and the differential states in the controller equations. The discrete design variables ($\boldsymbol{p_d}$) are the number of stages ($N_s$), feed stage location ($n_f$), side stream stage location ($n_s$), and equipment sizes. The real-valued design variables ($\boldsymbol{p_r}$) are the reflux rate ($L_1$), and all the controller tuning parameters. The remaining variables are all algebraic variables ($\boldsymbol{y}$). The equations presented in this section were implemented in a software tool called CasADi (Andersson et al., 2019) using its Python front-end.

## 4. The boundary value problem formulation

As an IVP, the solution of the hybrid model describing the semicontinuous distillation process is obtained by carrying out numerical integration from $t_0$ where the values of $\boldsymbol{z}(t_0(\boldsymbol{p_d}, \boldsymbol{p_r}), \boldsymbol{p_d}, \boldsymbol{p_r})$, and $\boldsymbol{y}(t_0(\boldsymbol{p_d}, \boldsymbol{p_r}), \boldsymbol{p_d}, \boldsymbol{p_r})$ are specified. The integrator then uses an event detection algorithm (which is a bisection algorithm) during an integration step for finding the location of the state-dependent events, which trigger the mode transition to some desired degree of tolerance (Aspen Plus® Dynamics; Barton, 1992). After detecting the location of an event where the instantaneous mode transition occurs, the DAE equation system is reinitialized, and then the integration is continued (Aspen Plus® Dynamics; Barton, 1992).

In a general boundary value problem with DAEs (DAE-BVP), the solution of the DAE is specified at more than one point, called the multi-point DAE-BVPs, by specifying conditions called the boundary conditions at these points (Ascher and Petzold, 1998; Lamour et al., 2015). However, typically, in most applications, the boundary conditions are just specified at two points (boundaries), which are called the two-point DAE-BVPs (Ascher and Petzold, 1998; Lamour et al., 2015). Boundary conditions that enforce time-periodic behaviour are non-separable, which

means that the conditions specified at the boundaries are not independent (Lamour et al., 2015). For a semi-explicit index-1 DAE, it is enough to enforce the boundary conditions only on the differential states because the algebraic states can be uniquely determined using the algebraic equations based on the values of the differential states (Lamour et al., 2015).

$$\boldsymbol{z}(t, \boldsymbol{p_d}, \boldsymbol{p_r}) - \boldsymbol{z}(t + \Gamma(\boldsymbol{p_d}, \boldsymbol{p_c}), \boldsymbol{p_d}, \boldsymbol{p_r}) = \mathbf{0} \tag{24}$$

where $\Gamma(\boldsymbol{p_d}, \boldsymbol{p_c})$ is the period of oscillation. This formulation was extended to hybrid systems by Khan et al., 2011, where the authors provided rigorous mathematical definitions. Based on their framework, the time-periodic boundary condition for semicontinuous distillation is defined as follows,

$$\boldsymbol{z}^{(\mu_1)}(t_0(\boldsymbol{p_d}, \boldsymbol{p_r}), \boldsymbol{p_d}, \boldsymbol{p_r}) - \boldsymbol{z}^{(\mu_1)}(t_3(\boldsymbol{p_d}, \boldsymbol{p_r}), \boldsymbol{p_d}, \boldsymbol{p_r}) = \mathbf{0} \tag{25}$$

where $t_0(\boldsymbol{p_d}, \boldsymbol{p_r}) \coloneqq 0$, and we consider that the processing starts at the beginning of the mode $\mu_1$, which is the separating mode. The BVP of the hybrid model of the semicontinuous distillation system (hybrid-BVP) can thus be defined as follows,

$$\begin{aligned}
\dot{\boldsymbol{z}}^{(\mu_i)}(t, \boldsymbol{p_d}, \boldsymbol{p_r}) = & \begin{bmatrix} \boldsymbol{\Psi}_{cc}\left(\boldsymbol{z}^{(\mu_i)}, \boldsymbol{y}^{(\mu_i)}(t, \boldsymbol{p_d}, \boldsymbol{p_r}), \boldsymbol{p_d}, \boldsymbol{p_r}\right) \\ \boldsymbol{\Psi}_{mv}^{(\mu_i)}\left(\boldsymbol{z}^{(\mu_i)}, \boldsymbol{y}^{(\mu_i)}(t, \boldsymbol{p_d}, \boldsymbol{p_r}), \boldsymbol{p_d}, \boldsymbol{p_r}\right) \end{bmatrix} \\
\mathbf{0} = & \begin{bmatrix} \boldsymbol{\Phi}_{cc}\left(\boldsymbol{z}^{(\mu_i)}, \boldsymbol{y}^{(\mu_i)}(t, \boldsymbol{p_d}, \boldsymbol{p_r}), \boldsymbol{p_d}, \boldsymbol{p_r}\right) \\ \boldsymbol{\Phi}_{mv}^{(\mu_i)}\left(\boldsymbol{z}^{(\mu_i)}, \boldsymbol{y}^{(\mu_i)}(t, \boldsymbol{p_d}, \boldsymbol{p_r}), \boldsymbol{p_d}, \boldsymbol{p_r}\right) \end{bmatrix} \qquad i = \{1, 2, 3\} \\
0 = & \ \Omega_{\mu_1}^{\mu_2}(t, \boldsymbol{p_d}, \boldsymbol{p_r}) \\
0 = & \ \Omega_{\mu_2}^{\mu_3}(t, \boldsymbol{p_d}, \boldsymbol{p_r}) \\
0 = & \ \Omega_{\mu_3}^{\mu_1}(t, \boldsymbol{p_d}, \boldsymbol{p_r}) \\
0 = & \ \boldsymbol{\Theta}_{\boldsymbol{z}\,\mu_i}^{\mu_j}(t, \boldsymbol{p_d}, \boldsymbol{p_r}) \\
0 = & \ \boldsymbol{\Theta}_{\boldsymbol{y}\,\mu_i}^{\mu_j}(t, \boldsymbol{p_d}, \boldsymbol{p_r}) \\
0 = & \ \boldsymbol{z}^{(\mu_1)}(t_0(\boldsymbol{p_d}, \boldsymbol{p_r}), \boldsymbol{p_d}, \boldsymbol{p_r}) - \boldsymbol{z}^{(\mu_1)}(t_3(\boldsymbol{p_d}, \boldsymbol{p_r}), \boldsymbol{p_d}, \boldsymbol{p_r})
\end{aligned} \tag{26}$$

where,

$\boldsymbol{z}^{(\mu_1)}(t_0(\boldsymbol{p_d}, \boldsymbol{p_r}), \boldsymbol{p_d}, \boldsymbol{p_r}) = \boldsymbol{z_0}(\boldsymbol{p_d}, \boldsymbol{p_r})$

The value of $\boldsymbol{z_0}(\boldsymbol{p_d}, \boldsymbol{p_r})$ is particularly picked to coincide with the location of the event that satisfies the transition condition $\Omega_{\mu_3}^{\mu_1}(t, \boldsymbol{p_d}, \boldsymbol{p_r})$, i.e., $h_{mv}^{(\mu_1)}(t_0(\boldsymbol{p_d}, \boldsymbol{p_r}), \boldsymbol{p_d}, \boldsymbol{p_r}) = h_{mv}^{u}$. This selection, called the phase-locking condition (Seydel, 2010), limits the initial state value to a particular point on the periodic orbit (Khan et al., 2011). As a consequence of the periodic boundary condition, $h_{mv}^{(\mu_1)}(t_3(\boldsymbol{p_d}, \boldsymbol{p_r}), \boldsymbol{p_d}, \boldsymbol{p_r})$ is therefore implicitly specified.

### 4.1 Single shooting method for obtaining the solution of the hybrid-BVP

The shooting method is an ideal way of solving BVPs of ordinary differential equations and differential-algebraic equations. The main philosophy behind the shooting method is to transform the BVP to a family of IVPs, whose initial values are unknown. The goal is to find the initial value that satisfies the boundary conditions. In this paper, we use this method, specifically, the single shooting method for solving the hybrid-BVP (15).

We treated the hybrid-BVP as having four independent DAE-BVPs linked together through the transition functions $\boldsymbol{\Theta}_{\boldsymbol{z}}^{\mu_j}_{\mu_i}(t, \boldsymbol{p_d}, \boldsymbol{p_r})$ and $\boldsymbol{\Theta}_{\boldsymbol{y}}^{\mu_j}_{\mu_i}(t, \boldsymbol{p_d}, \boldsymbol{p_r})$ to apply the single shooting method. The four DAEs correspond to the dynamic models of the system in the four epochs defined in section 3. Since we pick the initial value to coincide with the event location, the time interval of the fourth epoch is zero, and thus we can safely ignore this epoch. Hence, three DAE-BVPs are mathematically defined here,

**DAE-BVP 1**:

$$\begin{aligned}
\dot{\boldsymbol{z}}^{(\mu_1)}(t, \boldsymbol{p_d}, \boldsymbol{p_r}) = & \begin{bmatrix} \boldsymbol{\Psi}_{cc}\left(\boldsymbol{z}^{(\mu_1)}, \boldsymbol{y}^{(\mu_1)}(t, \boldsymbol{p_d}, \boldsymbol{p_r}), \boldsymbol{p_d}, \boldsymbol{p_r}\right) \\ \boldsymbol{\Psi}_{mv}^{(\mu_1)}\left(\boldsymbol{z}^{(\mu_1)}, \boldsymbol{y}^{(\mu_1)}(t, \boldsymbol{p_d}, \boldsymbol{p_r}), \boldsymbol{p_d}, \boldsymbol{p_r}\right) \end{bmatrix} \\
\boldsymbol{0} = & \begin{bmatrix} \boldsymbol{\Phi}_{column}\left(\boldsymbol{z}^{(\mu_1)}, \boldsymbol{y}^{(\mu_1)}(t, \boldsymbol{p_d}, \boldsymbol{p_r}), \boldsymbol{p_d}, \boldsymbol{p_r}\right) \\ \boldsymbol{\Phi}_{mv}^{(\mu_1)}\left(\boldsymbol{z}^{(\mu_1)}, \boldsymbol{y}^{(\mu_1)}(t, \boldsymbol{p_d}, \boldsymbol{p_r}), \boldsymbol{p_d}, \boldsymbol{p_r}\right) \end{bmatrix} \\
x_{mv,IVC}^{desired} = & \; x_{mv,IVC}^{(\mu_1)}(t_1(\boldsymbol{p_d}, \boldsymbol{p_r}), \boldsymbol{p_d}, \boldsymbol{p_r}) \\
\boldsymbol{z_0}(\boldsymbol{p_d}, \boldsymbol{p_r}) = & \; \boldsymbol{z}^{(\mu_1)}(t_0(\boldsymbol{p_d}, \boldsymbol{p_r}), \boldsymbol{p_d}, \boldsymbol{p_r}) \\
\boldsymbol{y_0}(\boldsymbol{p_d}, \boldsymbol{p_r}) = & \; \boldsymbol{y}^{(\mu_1)}(t_0(\boldsymbol{p_d}, \boldsymbol{p_r}), \boldsymbol{p_d}, \boldsymbol{p_r})
\end{aligned} \tag{27}$$

where $\boldsymbol{y_0}(\boldsymbol{p_d}, \boldsymbol{p_r})$ is the value of the algebraic state that is consistent with the DAE at $t_0(\boldsymbol{p_d}, \boldsymbol{p_r})$. This DAE-BVP is applicable in the time interval $[t_0(\boldsymbol{p_d}, \boldsymbol{p_r}), t_1(\boldsymbol{p_d}, \boldsymbol{p_r})]$.

**DAE-BVP 2**:

$$\begin{aligned}
\dot{\boldsymbol{z}}^{(\mu_2)}(t, \boldsymbol{p_d}, \boldsymbol{p_r}) = & \begin{bmatrix} \boldsymbol{\Psi}_{cc}\left(\boldsymbol{z}^{(\mu_2)}, \boldsymbol{y}^{(\mu_2)}(t, \boldsymbol{p_d}, \boldsymbol{p_r}), \boldsymbol{p_d}, \boldsymbol{p_r}\right) \\ \boldsymbol{\Psi}_{mv}^{(\mu_1)}\left(\boldsymbol{z}^{(\mu_2)}, \boldsymbol{y}^{(\mu_2)}(t, \boldsymbol{p_d}, \boldsymbol{p_r}), \boldsymbol{p_d}, \boldsymbol{p_r}\right) \end{bmatrix} \\
\boldsymbol{0} = & \begin{bmatrix} \boldsymbol{\Phi}_{cc}\left(\boldsymbol{z}^{(\mu_2)}, \boldsymbol{y}^{(\mu_2)}(t, \boldsymbol{p_d}, \boldsymbol{p_r}), \boldsymbol{p_d}, \boldsymbol{p_r}\right) \\ \boldsymbol{\Phi}_{mv}^{(\mu_2)}\left(\boldsymbol{z}^{(\mu_2)}, \boldsymbol{y}^{(\mu_2)}(t, \boldsymbol{p_d}, \boldsymbol{p_r}), \boldsymbol{p_d}, \boldsymbol{p_r}\right) \end{bmatrix} \\
h_{mv}^{l} = & \; h_{mv}^{(\mu_2)}(t_2(\boldsymbol{p_d}, \boldsymbol{p_r}), \boldsymbol{p_d}, \boldsymbol{p_r}) \\
\boldsymbol{z}^{(\mu_1)}(t_1(\boldsymbol{p_d}, \boldsymbol{p_r}), \boldsymbol{p_d}, \boldsymbol{p_r}) = & \; \boldsymbol{z}^{(\mu_2)}(t_1(\boldsymbol{p_d}, \boldsymbol{p_r}), \boldsymbol{p_d}, \boldsymbol{p_r})
\end{aligned}$$

$$\boldsymbol{y}^{(\mu_1)}(t_1(\boldsymbol{p_d},\boldsymbol{p_r}),\boldsymbol{p_d},\boldsymbol{p_r}) = \quad \boldsymbol{y}^{(\mu_2)}(t_1(\boldsymbol{p_d},\boldsymbol{p_r}),\boldsymbol{p_d},\boldsymbol{p_r}) \tag{28}$$

This DAE-BVP is applicable in the time interval $[t_1(\boldsymbol{p_d},\boldsymbol{p_r}), t_2(\boldsymbol{p_d},\boldsymbol{p_r})]$.

**DAE-BVP 3**:

$$\dot{\boldsymbol{z}}^{(\mu_3)}(t,\boldsymbol{p_d},\boldsymbol{p_r}) = \quad \begin{bmatrix} \boldsymbol{\Psi}_{cc}\left(\boldsymbol{z}^{(\mu_3)},\boldsymbol{y}^{(\mu_3)}(t,\boldsymbol{p_d},\boldsymbol{p_r}),\boldsymbol{p_d},\boldsymbol{p_r}\right) \\ \boldsymbol{\Psi}_{mv}^{(\mu_3)}\left(\boldsymbol{z}^{(\mu_3)},\boldsymbol{y}^{(\mu_3)}(t,\boldsymbol{p_d},\boldsymbol{p_r}),\boldsymbol{p_d},\boldsymbol{p_r}\right) \end{bmatrix}$$

$$\boldsymbol{0} = \quad \begin{bmatrix} \boldsymbol{\Phi}_{cc}\left(\boldsymbol{z}^{(\mu_3)},\boldsymbol{y}^{(\mu_3)}(t,\boldsymbol{p_d},\boldsymbol{p_r}),\boldsymbol{p_d},\boldsymbol{p_r}\right) \\ \boldsymbol{\Phi}_{mv}^{(\mu_3)}\left(\boldsymbol{z}^{(\mu_3)},\boldsymbol{y}^{(\mu_3)}(t,\boldsymbol{p_d},\boldsymbol{p_r}),\boldsymbol{p_d},\boldsymbol{p_r}\right) \end{bmatrix}$$

$$h_{mv}^{u} = \quad h_{mv}^{(\mu_3)}(t_3(\boldsymbol{p_d},\boldsymbol{p_r}),\boldsymbol{p_d},\boldsymbol{p_r})$$

$$\boldsymbol{z}^{(\mu_2)}(t_2(\boldsymbol{p_d},\boldsymbol{p_r}),\boldsymbol{p_d},\boldsymbol{p_r}) = \quad \boldsymbol{z}^{(\mu_3)}(t_2(\boldsymbol{p_d},\boldsymbol{p_r}),\boldsymbol{p_d},\boldsymbol{p_r})$$

$$\boldsymbol{y}^{(\mu_2)}(t_2(\boldsymbol{p_d},\boldsymbol{p_r}),\boldsymbol{p_d},\boldsymbol{p_r}) = \quad \boldsymbol{y}^{(\mu_3)}(t_2(\boldsymbol{p_d},\boldsymbol{p_r}),\boldsymbol{p_d},\boldsymbol{p_r})$$

$$\boldsymbol{z_0}(\boldsymbol{p_d},\boldsymbol{p_r}) = \quad \boldsymbol{z}^{(\mu_3)}(t_3(\boldsymbol{p_d},\boldsymbol{p_r}),\boldsymbol{p_d},\boldsymbol{p_r}) \tag{29}$$

This DAE-BVP is applicable in the time interval $[t_2(\boldsymbol{p_d},\boldsymbol{p_r}), t_3(\boldsymbol{p_d},\boldsymbol{p_r})]$.

The single shooting method is an iterative procedure that involves integration and solving a system of non-linear algebraic equations. In brief, in this method, first, the DAEs in (27), (28), and (29) are integrated numerically to obtain solutions $\boldsymbol{z}^{(\mu_i)}(t,\boldsymbol{p_d},\boldsymbol{p_r})$ and $\boldsymbol{y}^{(\mu_i)}(t,\boldsymbol{p_d},\boldsymbol{p_r})$, for $i = \{1,2,3\}$, that satisfy the guessed initial conditions $\boldsymbol{z_0}(\boldsymbol{p_d},\boldsymbol{p_r})$ and $\boldsymbol{y_0}(\boldsymbol{p_d},\boldsymbol{p_r})$. These solutions are used to solve a system of non-linear algebraic equations formed by the boundary conditions imposed at the end of the time interval in which the DAE-BVP system is valid to improve the initial guess. The process is repeated until the desired convergence tolerance is obtained. The initial guess for $\boldsymbol{z_0}(\boldsymbol{p_d},\boldsymbol{p_r})$ and $\boldsymbol{y_0}(\boldsymbol{p_d},\boldsymbol{p_r})$ was selected such that it is the state of the hypothetical continuous distillation system described in the introduction section, for chosen $\boldsymbol{p_d}$ and $\boldsymbol{p_r}$ of the semicontinuous distillation system. Based on our experience in simulating semicontinuous distillation systems, convergence to a limit cycle is generally possible when this state is used as the initial state at $t = 0$.

To have a fixed horizon of integration ($[0,1]$) during the numerical integration process, some well-know tricks were applied to reformulate the DAEs (Ascher and Petzold, 1998). Specifically, we apply a change of variable by changing the independent variable $t$ to $\tau$. The change of variable for the three DAE-BVPs is as follows,

**DAE-BVP 1**: $\tau = {}^{t}/_{t_1(\boldsymbol{p_d},\boldsymbol{p_r})}$ (30)

**DAE-BVP 2**: $\tau = {}^{t}/_{t_2(\boldsymbol{p_d},\boldsymbol{p_r})}$ (31)

**DAE-BVP 3**: $\tau = {}^{t}/_{t_3(\boldsymbol{p_d},\boldsymbol{p_r})}$ (32)

The differential equation systems of the three BVPs were each augmented by adding the following differential equations because of the reformulation,

**DAE-BVP 1**: $\frac{dt_1(\boldsymbol{p_d},\boldsymbol{p_r})}{d\tau} = 0$ (33)

**DAE-BVP 2**:$\frac{dt_2(\boldsymbol{p_d},\boldsymbol{p_r})}{d\tau} = 0$ (34)

**DAE-BVP 3**: $\frac{dt_3(\boldsymbol{p_d},\boldsymbol{p_r})}{d\tau} = 0$ (35)

Appropriate modifications were also made to the differential equation part of the differential-algebraic equation systems to change $\frac{d\boldsymbol{z}^{(\mu_i)}}{dt}$ to $\frac{d\boldsymbol{z}^{(\mu_i)}}{d\tau}$.

## 5. Application of the single shooting method

The single shooting method for semicontinuous distillation design that was described in the previous section was applied to two case studies, both involving the separation of hexane, heptane, and octane. Details of the two case studies are provided in the table (Table 2). The properties of the components in the liquid mixture ($T_c^{cr}$, $P_c^{cr}$, $Z_c^{Ra}$, $A_c$, $B_c$, $C_c$, $D_c$, $E_c$) were taken from Aspen Physical Property database and Perry and Green, 2013. The initial guesses of the differential states and the algebraic states for chosen values of $N_s$, $n_f$, $n_s$, $x_{1,HVC}^{desired}$, and $x_{N_s,LVC}^{desired}$ for the two case studies, were obtained by simulating the hypothetical continuous distillation system in Aspen Plus V10. The values of the number of trays and reflux ratio values can be obtained from the modified Fenske-Underwood equations (Phimister and Seider, 2000). The cross-sectional areas of the tray ($A_{Tray}$), the reflux drum ($A_{reflux}$) and the sump ($A_{sump}$) were then used to calculate the liquid molar hold-ups on the stages based on the steady-state liquid flowrates leaving a stage.

Table 2: Some details of the systems (Case 1 and Case 2) used for demonstrating the application of the single shooting method. The system parameters in Case 2 were taken from Madabhushi and Adams, 2019.

| | **CASE 1** | **CASE 2** |
|---|---|---|
| **TERNARY MIXTURE** | Hexane, Heptane, Octane | Hexane, Heptane, Octane |
| $\boldsymbol{N_s}$ | 5 | 40 |
| $\boldsymbol{n_f}$ | 3 | 24 |
| $\boldsymbol{n_s}$ | 2 | 13 |
| $\boldsymbol{x_{1,HVC}^{desired}}$ | 0.65 | 0.95 |
| $\boldsymbol{x_{N_s,LVC}^{desired}}$ | 0.65 | 0.95 |
| $\boldsymbol{x_{mv,IVC}^{desired}}$ | 0.37 | 0.95 |

| | | |
|---|---|---|
| $\boldsymbol{A_{Tray}}$ ($m^2$) | 0.657 | 0.657 |
| $\boldsymbol{A_{reflux}}$ ($m^2$) | 0.805 | 2.350 |
| $\boldsymbol{A_{sump}}$ ($m^2$) | 0.368 | 2.746 |
| $\boldsymbol{P_1}$ (atm) | 1.0 | 1.0 |
| Stage pressure drop (atm) | 0.0805 | 0.0067 |

To find the initial guess of the transition times, $t_1(\boldsymbol{p_d}, \boldsymbol{p_r})$, $t_2(\boldsymbol{p_d}, \boldsymbol{p_r})$, and $t_3(\boldsymbol{p_d}, \boldsymbol{p_r})$ at which the transition conditions, $\Omega_{\mu_1}^{\mu_2}(t, \boldsymbol{p_d}, \boldsymbol{p_r})$, $\Omega_{\mu_2}^{\mu_3}(t, \boldsymbol{p_d}, \boldsymbol{p_r})$, and $\Omega_{\mu_3}^{\mu_1}(t, \boldsymbol{p_d}, \boldsymbol{p_r})$ are satisfied, the non-linear optimization solver IPOPT (Wächter and Biegler, 2006) was used. The objective function of the non-linear optimization problem solved using IPOPT is the Euclidean norm of the residuals of the transition conditions, while these conditions were posed as constraints of the optimization problem.

Once the initial guesses are obtained, to find the zeroes of the transition conditions and the periodicity conditions in (27), (28), (29) for improving the initial guess, the non-linear optimization solver IPOPT (Wächter and Biegler, 2006) was again used. The objective function of the non-linear optimization problem posed to IPOPT is the Euclidean norm of the residuals of these conditions, while the constraints are the conditions mentioned above. Additionally, this optimization problem includes decision variables bounds to ensure that a physically unrealistic solution is not obtained. The numerical integrator that is used to integrate the DAEs is IDAS (Hindmarsh et al., 2005), which is a differential-algebraic equation system integrator equipped with the forward and adjoint sensitivity analysis modules. CasADi software has control over the sensitivity analysis method that IDAS uses to compute the derivative information. Furthermore, in the checkpointing scheme that is used in the backward integration of the adjoint sensitivity system in IDAS, the number of steps per checkpoint was picked to be 1000 to ensure convergence. The optimization problem that is used to determine the initial guess of the mode transition times was solved to optimality with the default values of the IPOPT solver parameters. Below, we present the sketch of the algorithm for applying the single shooting method for semicontinuous distillation design.

**Algorithm: Single shooting method for semicontinuous distillation design**

*# User Inputs to Algorithm*

$\boldsymbol{p_d}$ ← **user_input** ($N_s$, $n_f$, $n_s$, $A_{Tray}$, $A_{reflux}$, $A_{sump}$)

$\boldsymbol{p_r}$ ← **user_input** ($L_1$, $\{\boldsymbol{K_{p,k}}\}$, $\{\boldsymbol{K_{I,k}}\}$) (where $\boldsymbol{k}$ = Distillate concentration controller, Bottoms concentration controller, Reflux Drum level controller, Sump level controller, Side stream flowrate controller)

**constants** ← **user_input** ($x_{1,HVC}^{desired}$, $x_{N_s,LVC}^{desired}$, $h_{reflux}^{desired}$, $h_{sump}^{desired}$, $x_{mv,IVC}^{desired}$, $h_{mv}^{l}$, $h_{mv}^{u}$, $\{Z_c^{Ra}, c = 1 \text{ to } 3\}$, $\{P_c^{cr}, c = 1 \text{ to } 3\}$, $\{T_c^{cr}, c = 1 \text{ to } 3\}$,

$\{A_c, c = 1 \text{ to } 3\}$, $\{B_c, c = 1 \text{ to } 3\}$, $\{C_c, c = 1 \text{ to } 3\}$,
$\{D_c, c = 1 \text{ to } 3\}$, $\{E_c, c = 1 \text{ to } 3\}$)

*# Set index $i$ to zero*
$i \leftarrow 0$

*# User guesses for the mode transition times based on user's experience*
**user_input** $(t_1^i, t_2^i, t_3^i)$

*# Set the initial guesses for the differential states associated with the integral term of the PI controllers ($I_k^i$) to zero*

**for $k$ =** {Distillate concentration controller, Bottoms concentration controller, Reflux Drum level controller, Sump level controller, Side stream flowrate controller}
$I_k^i \leftarrow 0$
**end for**

*# Solve non-linear algebraic equations of the hypothetical continuous distillation system analog to get the initial guesses for $m_{n,c}^i$, $m_{mv,c}^i$,* and $\boldsymbol{y_0^i(p_d, p_r)}$

$[m_{n,c}^i, m_{mv,c}^i, \boldsymbol{y_0^i(p_d, p_r)}]$ = **Solve** (*Hypothetical continuous distillation system equations*)

*# Set the initial guesses that will be used for solving the BVPs in the next step to be the results of the previous step*
$\boldsymbol{z_0(p_d, p_r)} \leftarrow (m_{n,c}^i, m_{mv,c}^i, I_k^i, t_1^i, t_2^i, t_3^i)$ (this is $\boldsymbol{z_0^i(p_d, p_r)}$)
$\boldsymbol{y_0(p_d, p_r)} \leftarrow \boldsymbol{y_0^i(p_d, p_r)}$

*# Solve the relaxed and reformulated boundary value problems DAEBVP-1, DAEBVP-2, DAEBVP-3 (which do not include periodic boundary conditions) to get a better initial guess for $t_1(\boldsymbol{p_d, p_r})$, $t_2(\boldsymbol{p_d, p_r})$,* and $t_3(\boldsymbol{p_d, p_r})$*. These new and better guesses will improve the convergence properties of the single shooting method in the final step.*

**while** norm (residual vector of mode transition conditions) > Desired tolerance

$[\boldsymbol{z^{(\mu_1)}(1, p_d, p_r)}, \boldsymbol{y^{(\mu_1)}(1, p_d, p_r)}]$ = **Integrate** (reformulated DAEBVP-1 DAEs, $\boldsymbol{z_0(p_d, p_r)}$, $\boldsymbol{y_0(p_d, p_r)}$)
$[\boldsymbol{z^{(\mu_2)}(1, p_d, p_r)}, \boldsymbol{y^{(\mu_2)}(1, p_d, p_r)}]$ = **Integrate** (reformulated DAEBVP-2 DAEs, $\boldsymbol{z^{(\mu_2)}(0, p_d, p_r)}$, $\boldsymbol{y^{(\mu_2)}(0, p_d, p_r)}$)
$[\boldsymbol{z^{(\mu_3)}(1, p_d, p_r)}, \boldsymbol{y^{(\mu_3)}(1, p_d, p_r)}]$ = **Integrate** (reformulated DAEBVP-3 DAEs, $\boldsymbol{z^{(\mu_3)}(0, p_d, p_r)}$, $\boldsymbol{y^{(\mu_3)}(0, p_d, p_r)}$)
$i \leftarrow i + 1$

$[t_1^i(\boldsymbol{p_d}, \boldsymbol{p_r}), t_2^i(\boldsymbol{p_d}, \boldsymbol{p_r}), t_3^i(\boldsymbol{p_d}, \boldsymbol{p_r})]$ = **Solve** $\left( \begin{bmatrix} \Omega_{\mu_1}^{\mu_2}(t, \boldsymbol{p_d}, \boldsymbol{p_r}) \\ \Omega_{\mu_3}^{\mu_1}(t, \boldsymbol{p_d}, \boldsymbol{p_r}) \\ \Omega_{\mu_2}^{\mu_3}(t, \boldsymbol{p_d}, \boldsymbol{p_r}) \end{bmatrix} = \boldsymbol{0} \right)$

$\boldsymbol{z_0}(\boldsymbol{p_d}, \boldsymbol{p_r}) \leftarrow \boldsymbol{z_0^i}(\boldsymbol{p_d}, \boldsymbol{p_r})$

$\boldsymbol{y_0}(\boldsymbol{p_d}, \boldsymbol{p_r}) \leftarrow \boldsymbol{y_0^i}(\boldsymbol{p_d}, \boldsymbol{p_r})$ (obtained based on $\boldsymbol{z_0^i}(\boldsymbol{p_d}, \boldsymbol{p_r})$)

**end while**

*# Single shooting*: *Solve the reformulated boundary value problems DAEBVP-1, DAEBVP-2, DAEBVP-3 to find the initial/final point of the limit cycle*

**while** norm (residual vector of boundary conditions) > Desired tolerance

$[\boldsymbol{z}^{(\mu_1)}(1, \boldsymbol{p_d}, \boldsymbol{p_r}), \boldsymbol{y}^{(\mu_1)}(1, \boldsymbol{p_d}, \boldsymbol{p_r})]$ = **Integrate** (reformulated DAEBVP-1 DAEs, $\boldsymbol{z_0}(\boldsymbol{p_d}, \boldsymbol{p_r}), \boldsymbol{y_0}(\boldsymbol{p_d}, \boldsymbol{p_r})$)

$[\boldsymbol{z}^{(\mu_2)}(1, \boldsymbol{p_d}, \boldsymbol{p_r}), \boldsymbol{y}^{(\mu_2)}(1, \boldsymbol{p_d}, \boldsymbol{p_r})]$ = **Integrate** (reformulated DAEBVP-2 DAEs, $\boldsymbol{z}^{(\mu_2)}(0, \boldsymbol{p_d}, \boldsymbol{p_r}), \boldsymbol{y}^{(\mu_2)}(0, \boldsymbol{p_d}, \boldsymbol{p_r})$)

$[\boldsymbol{z}^{(\mu_3)}(1, \boldsymbol{p_d}, \boldsymbol{p_r}), \boldsymbol{y}^{(\mu_3)}(1, \boldsymbol{p_d}, \boldsymbol{p_r})]$ = **Integrate** (reformulated DAEBVP-3 DAEs, $\boldsymbol{z}^{(\mu_3)}(0, \boldsymbol{p_d}, \boldsymbol{p_r}), \boldsymbol{y}^{(\mu_3)}(0, \boldsymbol{p_d}, \boldsymbol{p_r})$)

$i \leftarrow i + 1$

$[\boldsymbol{z_o^i}(\boldsymbol{p_d}, \boldsymbol{p_r})]$ = Solve $\left( \begin{bmatrix} \Omega_{\mu_1}^{\mu_2}(t, \boldsymbol{p_d}, \boldsymbol{p_r}) \\ \Omega_{\mu_3}^{\mu_1}(t, \boldsymbol{p_d}, \boldsymbol{p_r}) \\ \Omega_{\mu_2}^{\mu_3}(t, \boldsymbol{p_d}, \boldsymbol{p_r}) \\ \boldsymbol{z}^{(\mu_1)}(\boldsymbol{t_0}(\boldsymbol{p_d}, \boldsymbol{p_r}), \boldsymbol{p_d}, \boldsymbol{p_r}) - \boldsymbol{z}^{(\mu_1)}(\boldsymbol{t_3}(\boldsymbol{p_d}, \boldsymbol{p_r}), \boldsymbol{p_d}, \boldsymbol{p_r}) \end{bmatrix} = \boldsymbol{0} \right)$

$\boldsymbol{z_0}(\boldsymbol{p_d}, \boldsymbol{p_r}) \leftarrow \boldsymbol{z_0^i}(\boldsymbol{p_d}, \boldsymbol{p_r})$

$\boldsymbol{y_0}(\boldsymbol{p_d}, \boldsymbol{p_r}) \leftarrow \boldsymbol{y_0^i}(\boldsymbol{p_d}, \boldsymbol{p_r})$ (obtained based on $\boldsymbol{z_0^i}(\boldsymbol{p_d}, \boldsymbol{p_r})$)

**end while**

*# the limit cycle is now stored in* $\boldsymbol{z}(\boldsymbol{p_d}, \boldsymbol{p_r})$ *and* $\boldsymbol{y}(\boldsymbol{p_d}, \boldsymbol{p_r})$

Analysis of the results from many unsuccessful trials pointed to the observation that the side stream controller's integral term increases monotonically during the cycle. We manually reset this term to the initial value only at the beginning of a new cycle, because, overall, we found this to result in better system performance in terms of cost (Madabhushi and Adams, 2018). Because of this reason, the differential state associated with the side stream controller's integral term had to be dropped from the periodicity constraints enforced on DAE BVP-3. In Case 1, the optimization problem that was used to determine the point on the limit cycle was solved to optimality using IPOPT to a tolerance of 0.0001. The maximum absolute residual error of the differential state vector is less than this tolerance, while this error is slightly greater than tolerance (which is 0.0002) for the algebraic state vector.

When the algorithm failed to converge to the desired convergence tolerance, the controller tuning parameters and the reflux rate were varied until it is met using a trial and error method. Also, at the same time, by varying these design variables the top and bottoms product mass-averaged product purities were ensured to be met. In Figure 4, we present the two-dimensional phase plot between two differential states of Case 1. Convergence to tighter tolerances was found to be difficult, and after many tests, the reason could not be clearly surmised. But it is recognized that it could be due to a combination of numerical errors and the control system. To control the integration errors, the absolute and relative tolerance in the IDAS integrator were both chosen to be 0.00005. An initial step size of 0.001 and a maximum step size of 0.05 was selected. The mass-averaged product purities of the top and bottoms products were found to be 0.65.

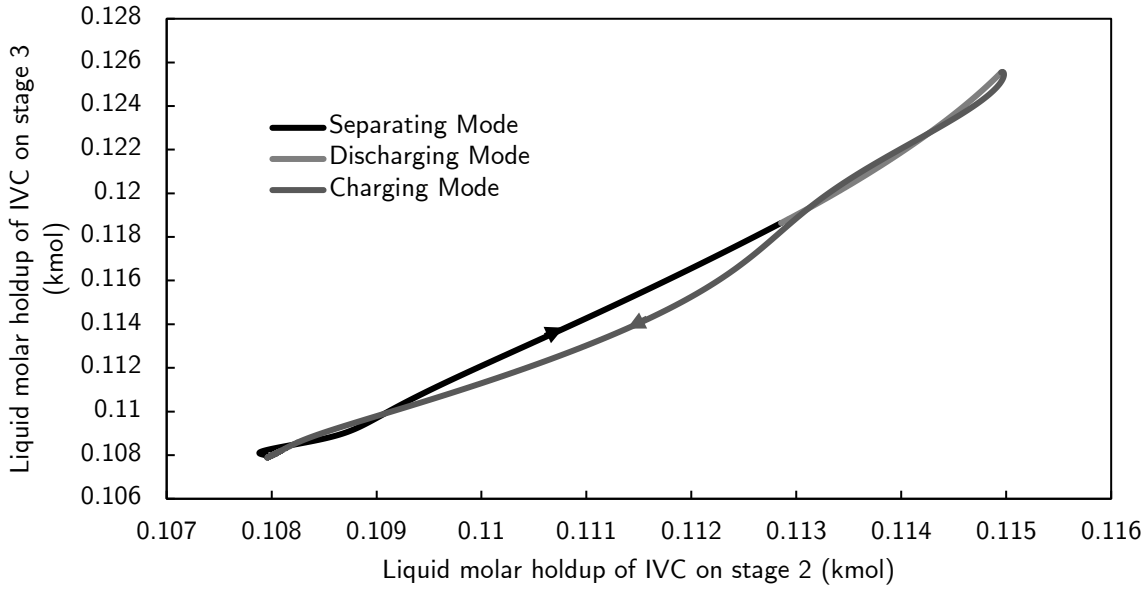


Figure 4: Two-dimensional phase plot illustrating the periodic orbit of the differential states $m_{2,1}(t)$ and $m_{3,1}(t)$ (in Case 1) which was obtained using the single shooting method.

Just as in Case 1, the controller tuning parameter values were varied to ensure convergence of the optimization problem that was used to determine the point on the limit cycle in Case-2. This problem was solved using IPOPT by using a convergence tolerance of 0.0001. The maximum absolute residual error of the differential state vector is less than this tolerance (0.00003), while this error is greater than tolerance (0.003) for the algebraic state vector. However, after analyzing the relative residual error of the algebraic state vector, which is 0.000008, we found that the result is acceptable for all practical purposes. The mass-averaged product purities of the top and bottoms products were found to be 0.96 and 0.951, respectively. The phase plot illustrating the periodic behaviour of this system is presented in Figure 5.

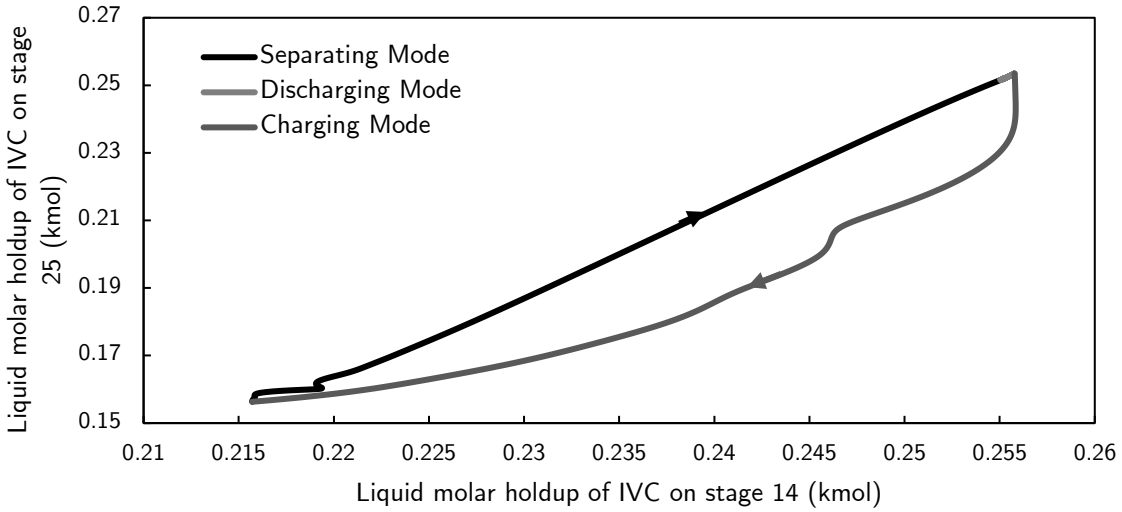


Figure 5: Two-dimensional phase plot illustrating the periodic orbit of the differential states $m_{14,1}(t)$ and $m_{25,1}(t)$ (in Case 2) which was obtained using the single shooting method.

A comparison of the phase plot in Figure 5 with the the phase plot obtained from Aspen Plus Dynamics when using a rigorous model illustrates important differences (Figure 6). From a cursory glance, qualitatively the shape and orientation of the cycles obtained from Aspen Plus Dynamics and the limit cycle found in this study is almost similar, although quantitatively they are very different. Further analysis points that this could be because of two reasons, firstly, a rigorous column model is used in Aspen to model the system as opposed to a simple model that was used in this study. Secondly, we observed that the for a certain period during the cycle the rate of material is recycled to the middle-vessel through the side stream is less in case of the Aspen model when compared to the CasADi (simple) model used in this study (Figure 7). Therefore, there is less material holdup in the column leading to a smaller span of the limit cycle (Figure 6) found in the current study.

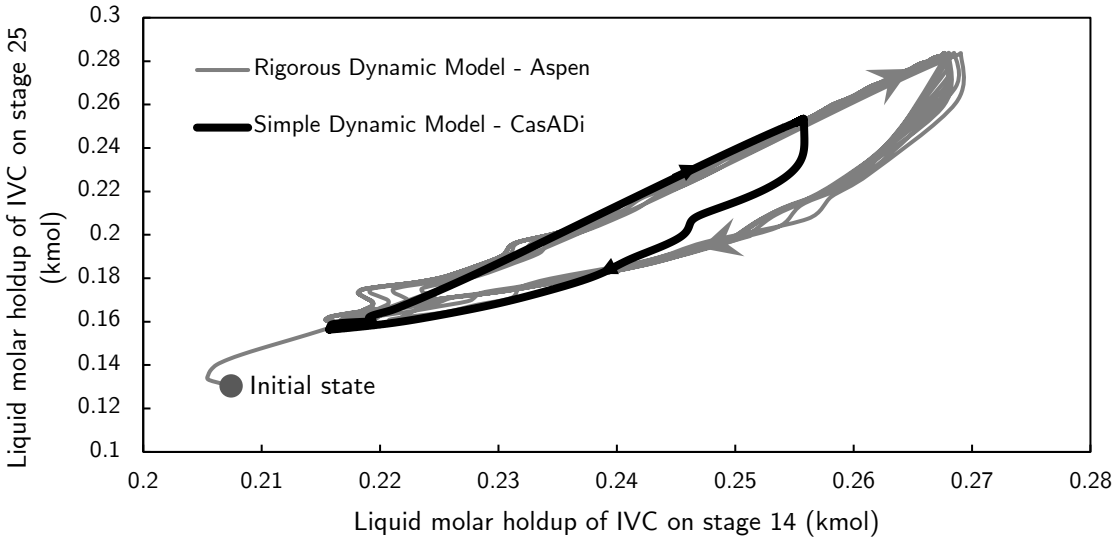


Figure 6: Plot illustrating the quantitative and qualitative differences in the cycles found using the rigorous model (10 cycles) and the limit cycle found using the simple model and the single shooting method.

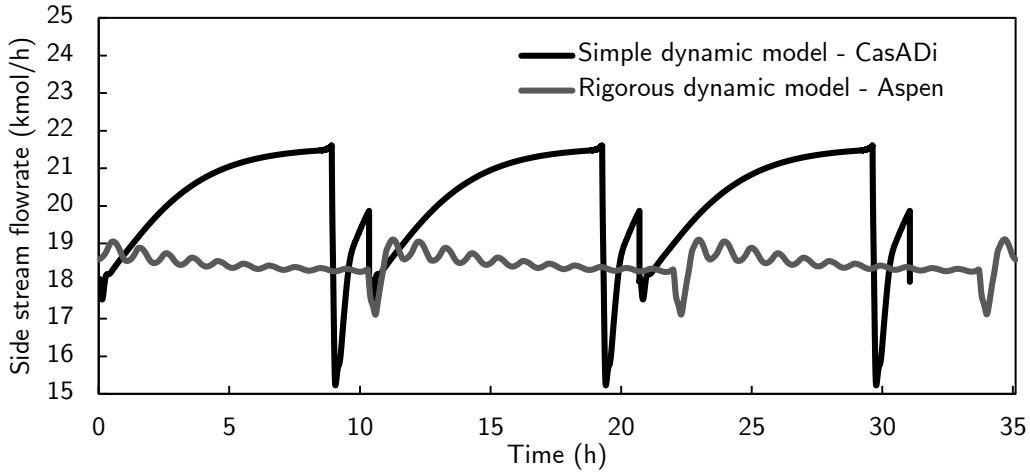


Figure 7: Plot illustrating the quantitative difference in the side stream flowrates.

A plot showing the dynamics of the mole fraction of the components in the middle vessel is presented as Figure 8. Since the focus of this article is to demonstrate the application of the algorithm for design, we do not check the feasibility of the column operation in terms of meeting the flooding, weeping, and weir loading limits in the cases. However, these limits can be easily met by adjusting the cross-sectional area of the trays ($A_{Tray}$) in the distillation column. Most importantly, the side stream pump and valve can be sized after the designing the system based on the trajectory of the side stream flowrate, which is in stark contrast to the backstepping design methodology.

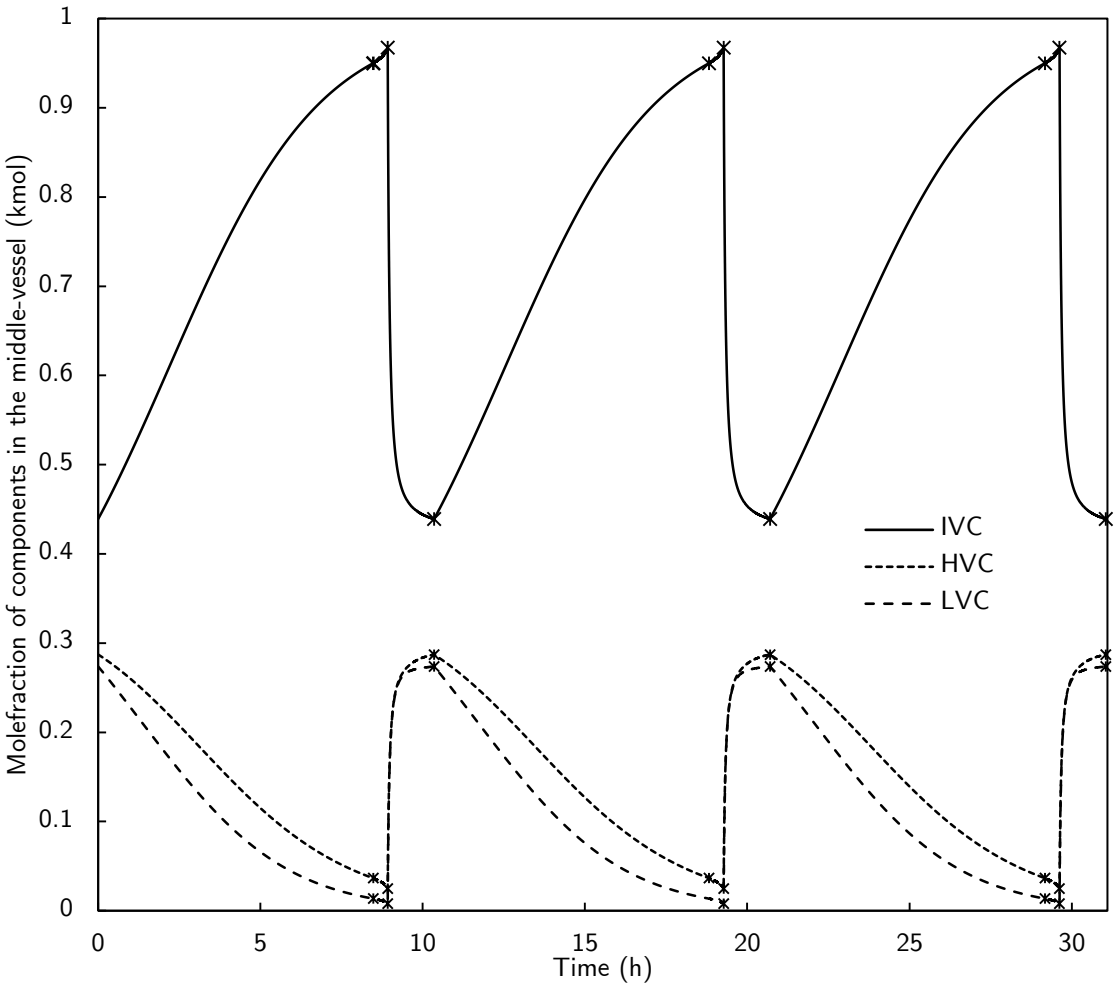


Figure 8: Plot illustrating the mole fraction dynamics of the components in the middle vessel. The stars indicate the time at which mode transitions occur.

## 6. Conclusion and Future work

This paper presents the application of the single shooting method for use in the design of semicontinuous distillation of ternary mixtures. The existing design methodologies were based on heuristics, and neither provided a guarantee on the optimality of the design obtained nor helped in identifying the precise location of the limit cycle. In this article, the proposed algorithm was applied to two case studies, both involving the separation of hexane, heptane, and octane, to demonstrate its use in determining the location of the limit cycle accurately to the desired convergence tolerance. We envision to incorporate the proposed single shooting algorithm in a gradient-based optimization framework to find the optimal semicontinuous distillation design for the separation of a given mixture in the future. The python files of this study are available on LAPSE: http://psecommunity.org/LAPSE:2020.0029.

**Acknowledgment**

This work was supported by the McMaster Advanced Control Consortium (MACC) and the Ontario Research Fund, grant number RE09-058.

**Nomenclature**

*Abbreviations*

| | |
|---|---|
| HVC | High volatile component |
| LVC | Low volatile component |
| IVC | Intermediate volatile component |
| DAE | Differential Algebraic Equations |
| SP | Setpoint |
| PV | Process variable |
| DAE-BVP | Boundary value problem involving differential-algebraic equations |
| hybrid-BVP | Boundary value problem involving the hybrid model |

*Greek symbols*

| | |
|---|---|
| $\rho_n^{liq}$ | Density of liquid on tray $n$ |
| $\theta_i$ | $i^{\text{th}}$ epoch in the hybrid model |
| $\mu_i$ | Mode $i$ in the hybrid model |
| $\boldsymbol{\Psi}_{cc}$ | Differential equations of the column and the control system |
| $\boldsymbol{\Phi}_{cc}$ | Algebraic equations of the column and the control system |
| $\boldsymbol{\Psi}_{mv}^{(\mu_i)}$ | Differential equations of the middle-vessel in mode $\mu_i$ |
| $\boldsymbol{\Phi}_{mv}^{(\mu_i)}$ | Algebraic equations of the middle-vessel in mode $\mu_i$ |
| $\Omega_{\mu_i}^{\mu_j}$ | The condition required to transition from mode $\mu_i$ to mode $\mu_j$ at $t_i$ |
| $\boldsymbol{\Theta}_{\boldsymbol{z}}{}_{\mu_i}^{\mu_j}$ | Transition functions of the hybrid model related to the differential variables |
| $\boldsymbol{\Theta}_{\boldsymbol{y}}{}_{\mu_i}^{\mu_j}$ | Transition functions of the hybrid model related to the algebraic variables |
| $\zeta$ | Binary number |
| $\varsigma$ | Binary number |

| | |
|---|---|
| $\alpha$ | Binary Number |
| $\beta$ | Binary Number |
| $\Gamma$ | Period of oscillation |
| $\tau$ | Dummy time variable |

*Other Symbols*

| | |
|---|---|
| $\boldsymbol{p_d}$ | Vector of design variables that take discrete values (discrete design variables) |
| $\boldsymbol{p_r}$ | Vector of design variables that take real values (real design variables) |
| $\boldsymbol{z}$ | Vector of differential state variables |
| $\boldsymbol{z_0}$ | Vector that specifies the initial state of the differential variables |
| $\boldsymbol{y}$ | Vector of algebraic state variables |
| $\boldsymbol{y_0}$ | Vector that specifies the initial state of the algebraic variables |
| $t_i$ | Time at which there is a switch in the model equations of the middle-vessel, $i = 1, 2, 3$ |
| $x_{1,HVC}(t)$ | Mole fraction of HVC on stage 1 |
| $x_{1,HVC}^{desired}$ | Desired mole fraction of HVC on stage 1 |
| $x_{mv,IVC}^{(\mu_1)}$ | Mole fraction of the intermediate volatile component in the middle-vessel in mode $\mu_1$ |
| $x_{mv,IVC}^{desired}$ | Desired purity value of the intermediate volatile component in the middle-vessel |
| $x_{N_s,LVC}(t)$ | Mole fraction of HVC on stage $N_s$ |
| $x_{N_s,LVC}^{desired}$ | Desired mole fraction of HVC on stage $N_s$ |
| $h_{mv}^{(\mu_2)}$ | Height of the liquid in the middle-vessel in mode $\mu_2$ |
| $h_v^l$ | Predetermined lower limit of height of the liquid in the middle-vessel |
| $h_{mv}^u$ | Predetermined upper limit of height of the liquid in the middle-vessel |
| $h_{reflux}(t))$ | Height of liquid in the reflux drum |
| $h_{reflux}^{desired}$ | Desired height of liquid in the reflux drum |
| $h_{sump}(t)$ | Height of liquid in the sump |
| $h_{sump}^{desired}$ | Desired height of liquid in the sump |

| | |
|---|---|
| $n$ | Stages |
| $n_f$ | Feed stage location |
| $n_s$ | Side stream stage |
| $c$ | Components |
| $N_s$ | Total number of stages |
| $m_{n,c}$ | Liquid molar holdup of component $c$ on stage $n$ |
| $M_n$ | Total molar holdup of liquid on stage $n$ |
| $l_{n,c}$ | Liquid flowrate of component $c$ leaving stage $n$ |
| $L_n$ | Total flowrate of liquid leaving stage $n$ |
| $v_{n,c}$ | Vapour molar flowrate of component $c$ entering stage $n$ |
| $V_n$ | Total flowrate of vapour leaving stage $n$ |
| $S$ | Side stream flowrate |
| $d$ | Distillate flowrate |
| $b$ | Bottoms flowrate |
| $F$ | Feed flowrate to the column |
| $V_{N_s}$ | Reboil rate |
| $d_c$ | Distillate molar flowrate of component $c$ leaving stage 1 |
| $f_c$ | Molar flowrate of component $c$ in the liquid feed |
| $s_c$ | Molar flowrate of component $c$ in the liquid side stream |
| $b_c$ | Bottoms molar flowrate of component $c$ leaving the stage $N_s$ |
| $K_c$ | Phase equilibrium ratio of component $c$ on stage $n$ |
| $y_{n,c}$ | Mole fraction of component $c$ in the vapour leaving stage $n$ |
| $x_{n,c}$ | Mole fraction of component $c$ in the liquid leaving stage $n$ |
| $T_n$ | Temperature of the stage $n$ |
| $P_n$ | Pressure of the stage $n$ |
| $A_c$ | Antoine parameter for component $c$ |
| $B_c$ | Antoine parameter for component $c$ |

| | |
|---|---|
| $C_c$ | Antoine parameter for component $c$ |
| $D_c$ | Antoine parameter for component $c$ |
| $E_c$ | Antoine parameter for component $c$ |
| $A_{Tray}$ | Tray cross-sectional area |
| $A_{reflux}$ | Cross-sectional area of the reflux drum |
| $A_{sump}$ | Cross-sectional area of the sump |
| $h_{weir}$ | Weir height |
| $L_{weir}$ | Weir length |
| $g$ | gravitational constant |
| $R_{gas}$ | Ideal gas constant |
| $T_c^{cr}$ | Critical temperature of component $c$ |
| $P_c^{cr}$ | Critical pressure of component $c$ |
| $Z_c^{Ra}$ | Rackett compressibility factor of component $c$ |
| $u$ | Manipulated variable |
| $u_{bias}$ | Controller bias |
| $K_p$ | Proportional gain |
| $K_i$ | Integral gain |
| $e$ | error (Setpoint – Process Variable value at time $t$) |
| $I$ | differential state of the integral term of the PI controller |
| $m_{mv,c}$ | Liquid molar holdup of component $c$ in the middle vessel |
| $f_{charge,c}$ | Liquid flowrate of component $c$ in the charging stream |
| $f_{discharge,c}$ | Liquid flowrate of component $c$ in the discharge stream |
| $T_\mu$ | Mode trajectory of the hybrid model |

## References


Adams II, T.A., Pascall, A., 2012. Semicontinuous Thermal Separation Systems. Chem. Eng. Technol. 35, 1153–1170. https://doi.org/10.1002/ceat.201200048

Adams, T.A., Pascall, A., 2012. Semicontinuous Thermal Separation Systems. Chem. Eng. Technol. https://doi.org/10.1002/ceat.201200048

Andersson, J.A.E., Gillis, J., Horn, G., Rawlings, J.B., Diehl, M., 2019. CasADi: a software framework for nonlinear optimization and optimal control. Math. Program. Comput. https://doi.org/10.1007/s12532-018-0139-4

Annakou, O., Mizsey, P., 1995. Rigorous investigation of heat pump assisted distillation. Heat Recover. Syst. CHP 15, 241–247. https://doi.org/10.1016/0890-4332(95)90008.

Ascher, U.M., Petzold, L.R., 1998. Computer methods for ordinary differential equations and differential-algebraic equations, Computer Methods for Ordinary Differential Equations and Differential-Algebraic Equations. https://doi.org/10.1137/1.9781611971392

Aspen Plus ® Dynamics [WWW Document]. AspenTech Inc. URL https://www.aspentech.com/en/products/pages/aspen-plus-dynamics (accessed 11.23.19a).

Bansal, V., Perkins, J.D., Pistikopoulos, E.N., 2002. A case study in simultaneous design and control using rigorous, mixed-integer dynamic optimization models. Ind. Eng. Chem. Res. https://doi.org/10.1021/ie010156n

Barton, P.I., 1992. The modelling and simulation of combined discrete/continuous processes. Imperial College London.

Barton, P.I., Lee, C.K., 2004. Design of process operations using hybrid dynamic optimization, in: Computers and Chemical Engineering. https://doi.org/10.1016/j.compchemeng.2003.09.015

Flatby, P., Skogestad, S., Lundström, P., 1994. Rigorous Dynamic Simulation of Distillation Columns Based on UV-Flash. IFAC Proc. Vol. https://doi.org/10.1016/s1474-6670(17)48161-4

Galán, S., Feehery, W.F., Barton, P.I., 1999. Parametric sensitivity functions for hybrid discrete/continuous systems. Appl. Numer. Math. https://doi.org/10.1016/S0168-9274(98)00125-1

Gani, R., Ruiz, C.A., Cameron, I.T., 1986. A generalized model for distillation columns-I. Model description and applications. Comput. Chem. Eng. https://doi.org/10.1016/0098-1354(86)85001-3

Green, D.W., Southard, M.Z., 2019. Perry's Chemical Engineers' Handbook, 9th Edition, McGraw-Hill Education.

Hindmarsh, A.C., Brown, P.N., Grant, K.E., Lee, S.L., Serban, R., Shumaker, D.E., Woodward,

C.S., 2005. SUNDIALS: Suite of nonlinear and differential/algebraic equation solvers. ACM Trans. Math. Softw. https://doi.org/10.1145/1089014.1089020

Khan, K.A., Saxena, V.P., Barton, P.I., 2011. Sensitivity analysis of limit-cycle oscillating hybrid systems. SIAM J. Sci. Comput. https://doi.org/10.1137/100804632

Khayet, M., 2011. Membranes and theoretical modeling of membrane distillation: A review. Adv. Colloid Interface Sci. 164, 56–88. https://doi.org/10.1016/J.CIS.2010.09.005

Kiss, A.A., 2014. Distillation technology - still young and full of breakthrough opportunities. J. Chem. Technol. Biotechnol. https://doi.org/10.1002/jctb.4262

Kiss, A.A., 2013. Advanced Distillation Technologies. John Wiley & Sons, Ltd, Chichester, UK. https://doi.org/10.1002/9781118543702

Lamour, R., März, R., Weinmüller, E., 2015. Boundary-Value Problems for Differential-Algebraic Equations: A Survey. https://doi.org/10.1007/978-3-319-22428-2_4

Madabhushi, P.B., Adams, T.A., 2019. Finding Better Limit Cycles of Semicontinuous Distillation. 1. Back Stepping Design Methodology. Ind. Eng. Chem. Res. 58, 16654–16666. https://doi.org/10.1021/acs.iecr.9b02639

Madabhushi, P.B., Adams, T.A., 2018. Side stream control in semicontinuous distillation. Comput. Chem. Eng. https://doi.org/10.1016/j.compchemeng.2018.09.002

Madabhushi, P.B., Medina, E.I.S., Adams, T.A., 2018. Understanding the dynamic behaviour of semicontinuous distillation, in: Computer Aided Chemical Engineering. https://doi.org/10.1016/B978-0-444-64235-6.50148-0

Maleta, V.N., Kiss, A.A., Taran, V.M., Maleta, B. V., 2011. Understanding process intensification in cyclic distillation systems. Chem. Eng. Process. Process Intensif. 50, 655–664. https://doi.org/10.1016/j.cep.2011.04.002

Meidanshahi, V., Adams, T.A., 2016. Integrated design and control of semicontinuous distillation systems utilizing mixed integer dynamic optimization. Comput. Chem. Eng. https://doi.org/10.1016/j.compchemeng.2016.03.022

Parker, T.S., Chua, L.O., Parker, T.S., Chua, L.O., 1989. Locating Limit Sets, in: Practical Numerical Algorithms for Chaotic Systems. https://doi.org/10.1007/978-1-4612-3486-9_5

Pascall, A., Adams, T.A., 2013. Semicontinuous separation of dimethyl ether (DME) produced from biomass. Can. J. Chem. Eng. https://doi.org/10.1002/cjce.21813

Perry, R.H., Green, D.W., 2013. Perry's Chemical Engineers' Handbook, 8th Edition, Journal of Chemical Information and Modeling. https://doi.org/10.1017/CBO9781107415324.004

Petlyuk, F.B., 2004. Distillation Theory and Its Application to Optimal Design of Separation Units. Cambridge University Press, Cambridge. https://doi.org/10.1017/CBO9780511547102

Phimister, J.R., Seider, W.D., 2000. Semicontinuous, middle-vessel distillation of ternary mixtures. AIChE J. https://doi.org/10.1002/aic.690460804

Prokopakis, G.J., Seider, W.D., 1983. Dynamic simulation of azeotropic distillation towers. AIChE J. https://doi.org/10.1002/aic.690290622

Seydel, R., 2010. Practical Bifurcation and Stability Analysis, Interdisciplinary Applied Mathematics. https://doi.org/10.1007/978-1-4419-1740-9

Skogestad, S., 1997. Dynamics and control of distillation columns - A critical survey. Model. Identif. Control. https://doi.org/10.4173/mic.1997.3.1

Toftegàrd, B., Clausen, C.H., Jørgensen, S.B., Abildskov, J., 2016. New Realization of Periodic Cycled Separation. Ind. Eng. Chem. Res. https://doi.org/10.1021/acs.iecr.5b03911

Wächter, A., Biegler, L.T., 2006. On the implementation of an interior-point filter line-search algorithm for large-scale nonlinear programming. Math. Program. https://doi.org/10.1007/s10107-004-0559-y

Wijesekera, K.N., Adams, T.A., 2015a. Semicontinuous Distillation of Quintenary and N-ary Mixtures. Ind. Eng. Chem. Res. https://doi.org/10.1021/acs.iecr.5b03219

Wijesekera, K.N., Adams, T.A., 2015b. Semicontinuous distillation of quaternary mixtures using one distillation column and two integrated middle vessels. Ind. Eng. Chem. Res. https://doi.org/10.1021/ie504584y